Old Dominion University Research Foundation

DEPARTMENT OF MECHANICAL ENGINEERING AND MECHANICS
COLLEGE OF ENGINEERING
OLD DOMINION UNIVERSITY
NORFOLK, VIRGINIA 23508

OPTIMAL CURE CYCLE DESIGN OF A RESIN-FIBER COMPOSITE LAMINATE

By

Jean W. Hou, Principal Investigator

and

Jeenson Sheen, Graduate Research Assistant

Final Report
For the period ended January 15, 1987

Prepared for the
National Aeronautics and Space Administration
Langley Research Center
Hampton, Virginia 23665

Under
Research Grant NAG-1-561
Robert M. Baucom, Technical Monitor
MD-Polymeric Materials Branch

July 1987

DEPARTMENT OF MECHANICAL ENGINEERING AND MECHANICS
COLLEGE OF ENGINEERING
OLD DOMINION UNIVERSITY
NORFOLK, VIRGINIA 23508

OPTIMAL CURE CYCLE DESIGN OF A RESIN-FIBER COMPOSITE LAMINATE

By

Jean W. Hou, Principal Investigator

and

Jeenson Sheen, Graduate Research Assistant

Final Report
For the period ended January 15, 1987

Prepared for the
National Aeronautics and Space Administration
Langley Research Center
Hampton, Virginia 23665

Under
Research Grant NAG-1-561
Robert M. Baucom, Technical Monitor
MD-Polymeric Materials Branch

Submitted by the
Old Dominion University Research Foundation
P. O. Box 6369
Norfolk, Virginia 23508

July 1987

ACKNOWLEDGEMENT

This research was completed under a project sponsored by the NASA-Langley Research Center, Hampton, Virginia, Grant No. NAG-1-561.

The authors wish to thank Mr. Robert M. Baucom, the technical monitor of the project, whose friendly guidance and encouragement made this research possible. The authors are also indebted to Dr. Tan H. Hou at the NASA Polymerical Material Branch for his help, valuable suggestions and comments.

OPTIMAL CURE CYCLE DESIGN OF A RESIN-FIBER COMPOSITE LAMINATE

Jean W. Hou* and Jeenson Sheen**
Old Dominion University, Norfolk, VA 23508

ABSTRACT

High performance polymeric composites have been experiencing increasing usage in the aerospace and automobile industries. Such materials are commonly composed of long or chopped fibers embedded in the thermosetting resin matrix. Changes in physical and chemical properties of such composite materials during the cure process are rather complex. Thus, it is not a trivial task to properly design a cure cycle (temperature and pressure profiles) for a cure process. The material should be cured uniformly and completely with the lowest void content; the temperature inside the laminate must not exceed some maximum value; and the cure process should be completed within the shortest amount of time. In the past, most cure cycle designs for newly developed composite systems are based upon the technique of trial and error. Such approach has long been recognized as costly and inefficient. Several simulation models have been developed recently for curing various epoxy matrix composites. This development represents a significant advancement in computerizing the cure cycle design. The next quest comes naturally to be the search of the "best" cure cycle for

---

* Assistant Professor, Department of Mechanical Engineering and Mechanics

** Graduate Student

a given composite laminate. The major thrust of this thesis is to study a unified Computer-Aided Design method for the cure cycle design that incorporates an optimal design technique with the analytical model of a composite cure process. The preliminary results of using this proposed method for optimal cure cycle design are reported and discussed in this thesis.

The cure process of interest is the compression molding of a polyester which is described by a diffusion-reaction system. The finite element method is employed to convert the initial-boundary value problem into a set of first order differential equations which are solved simultaneously by the DE program. The equations for thermal design sensitivities are derived by using the direct differentiation method and are solved by the DE program. Finally, a recursive quadratic programming algorithm with an active set strategy called a linearization method is used to optimally design the cure cycle, subjected to the given design performance requirements. The difficulty of casting the cure cycle design process into a proper mathematical form is recognized in this study. Various optimal design problems are formulated to address these aspects. The optimal solutions of these formulations are compared and discussed, and the major parameters which play major roles in the cure cycle design for a given composite laminate are identified.

TABLE OF CONTENTS

LIST OF TABLES

LIST OF FIGURES

LIST OF SYMBOLS

a_1	constant defined in Eq. (2.5)
a_2	constant defined in Eq. (2.5)
b	design variable
δb	perturbation of design variable
c	specific heat per unit mass of the composite J/g/K
C	coefficient matrix of N_i
d_1	constant defined in Eq. (2.5)
d_2	constant defined in Eq. (2.5)
f	function defined in Eq. (2.5)
h	one half thickness of the composite laminate
H(t)	heat evolved from the beginning of the reaction to some intermediate time t, J/g
Hr	total or ultimate heat of reaction during cure, J/g
k	thermal conductivity perpendicular to the plane of the composite (z-direction) W/m/°K
K_1	exponential function of Temperature defined in Eq. (2.5)
K_2	exponential function of Temperature defined in Eq. (2.5)
K	coefficient matrix of derivative of N_i
°K	temperature, Kelvin's Degree
ℓ	element length
$L_i(z)$	Linear interpolation function
m	constant defined in Eq. (2.5)
M	coefficient matrix of L_i
n	constant defined in Eq. (2.5)

$N_i(z)$	interpolation function
NE	number of element
$\underline{P}$	coefficient of Vector N_i
$\underline{Q}$	the rate of heat generated by the chemical reaction
R	universal gas constant
$\underline{R}$	the rate of load function of degree of cure
s	adjoint variable
t	time
T	temperature
T_o	initial temperature
T_c	control temperature
u	arbitrary testing function
v	arbitrary testing function
z	coordinate
λ	adjoint variable
α	degree of cure
α_o	degree of cure at outer surface
α_c	degree of cure at center plan
α_f	degree of cure at end of the cure cycle
ρ	density of the composite Kg/m^3
ψ_o	cost function
τ	total processing time
Γ	temperature, defined in Eq. (A.20)

Superscript

$\dot{}$	time derivative, i.e., $\dot{T} = \frac{dT}{dt}$
$'$	spatial derivative, i.e., $T' = \frac{dT}{dz}$
T	transpose, i.e., $\underline{p}^T$

Subscript

b	derivative with respect to the design variable, i.e., $\alpha_b = \frac{d\alpha}{db}$
Underline	vector, i.e., $\underline{p}$

CHAPTER 1

INTRODUCTION

Continuous fibers reinforced polymeric composites are used in many applications where high strength and low weight are important, such as in the aerospace industry. These composites are produced by embedding long or chopped high strength reinforcing fibers in a polymeric matrix. The matrix is important not only for transferring the load between fibers, but also for providing resistance to fracture in the composite and to distortions caused by the environment. One means to manufacture the composite laminate with continuous fiber is by combining unidirectionally oriented layers of fibers pre-impregnated with the uncured resin matrix and subsequently laying these up in the desired directions. This pre-impregnated composite precursor is called a prepreg. The composite parts and structures are then manufactured by curing the prepreg material. The cure process is accomplished by exposing the prepreg material to the elevated temperatures and pressures for a predetermined length of time. These elevated temperatures and pressures to which the prepreg material is subjected are referred to as the cure temperature and the cure pressure. The cure temperature provides the heat required for initiating and maintaining the chemical reactions in the resin during the cure process. Once the reactive matrix resin is heated, polymerization reactions start to occur. Polymer chains are extended and later crosslinked. Interactions between

the heat generated from the reactions and the heat transmitted by conduction and convection from the surrounding environment create a highly non-linear chemoviscosity profile which can dictate the resin flow characteristics during the cure process. After the resin is melted, by applying the cure pressure, the excess resin is squeezed out of the material. Consequently, the individual plies are consolidated and the vapor bubbles are compressed.

The magnitudes and durations of the cure temperature and the cure pressure applied during the cure process have significant consequences on the performance of the finished product. It is not a trivial task to design a proper cure cycle, that is, to determine a cure temperature and a cure pressure, due to the complex nature of the changes in physical and chemical properties of the composite material during the cure process. The composite material should be cured uniformly and completely with the lowest void content; temperatures inside the laminate must not exceed some maximum value; and the curing process should be completed in the shortest amount of time [1]. In the past, the cure cycle is selected empirically for newly developed composite systems. This trial and error type of empirical approach has long been recognized as costly and inefficient. The shortcomings of the empirical approach could be overcome, however, by the use of an analytical model. The recently developed model for curing epoxy matrix composites by Loos and Springer [1] represented a significant advancement in this aspect. The cure cycle can now be designed in a systematic manner to meet the major considerations mentioned earlier for various composite resin/fiber systems. As for the composite with chopped fibers, its manufacturing process [2] may be different from the one stated above.

However, the process can still be characterized similarly by the resin flow, chemical kinetics, chemoviscosity, etc. The considerations in the selection of the proper cure cycle are also very similar.

1.1 Objective and Motivation

As mentioned above, currently the method for the cure cycle design is a type of parametric study conducted by either physical experiments or numerical simulation [1,2]. This type of approach is costly and inefficient; and the true optimal condition may never be found. Therefore, the development of a unified and systematic approach to obtain an "optimal" cure cycle for a given composite material is needed. In this study, a unified Computer-Aided Design (CAD) method is proposed, which incorporates an optimal design technique with an analytical model of a composite cure process.

The optimization technique is not new and has been successfully applied to many transient problems in various disciplines such as mechanical systems [3], structural dynamics [4], chemical process control [5], and optimal control [6]. However, to the author's knowledge, the application of optimization technique to the cure cycle design has never been studied before. The goal of this study is to exploit the potential of applying the optimization technique to the cure cycle design.

As an initial attempt at this goal, this study is concentrated on the optimal design of the cure temperature only. The press molding process of a polyester [2] is used as an example. Various optimization formulations for the cure cycle design are suggested. Their optimal solutions are obtained by using the integrated computer program which is

developed for the simulation of a heat conduction model coupled with a chemo-kinetic model during the process and for the optimization of the cure cycle design. Those optimization formulations are evaluated based on their performances and merits. The experience gained from this study is very important and valuable for the further application of the proposed CAD approach to a more realistic composite manufacturing process.

1.2 Scope of the Present Work

The major contents of this thesis are Thermal Analysis, Thermal Design Sensitivity Analysis, and Optimal Cure Cycle Design. The considerations of the computational formulation of the reaction-diffusion system are reported in the next chapter. The finite element discretization is introduced to convert the initial-boundary value problem into a set of first order differential equations. These equations are then solved simultaneously by the DE program [7]. To verify the computational procedure, the numerical results of examples are compared with the analytical solutions or the solutions found in the literature [2,8,9,10].

In Chapter 3, two methods, the adjoint variable method and the direct differentiation method, have been studied for the thermal design sensitivity analysis. It is concluded that the direct differentiation method is superior to the adjoint variable method in terms of accuracy and physical interpretation. Once the information of design sensitivity is provided accurately, any gradient-based mathematical programming algorithm can be applied to generate the optimal design iteratively.

In Chapter 4, an iterative scheme is outlined to determine the best cure process. Numerical calculations are carried out by using the finite element method for analysis and a recursive quadratic programming technique for optimization. The results of the optimal cure cycle design for various formulations of objective functions are also presented.

Finally, remarks and conclusions of the present work are given in Chapter 5.

CHAPTER II

THERMAL ANALYSIS

One major step of manufacturing composite materials which consist of thermosetting resin matrix is using the elevated temperature and pressure to cure the materials. The analytical model of such a cure process is rather complicated. Such an analytical model should be able to address:

a) the heat transmission between the surrounding environment and the material,

b) the temperature distribution within the material,

c) the heat generated by the chemical reaction of the resin,

d) the phase change of the resin characterized by its chemoviscosity, and

e) the non-newtonian flow problem associated with the cure pressure and the liquidized resin.

Among others, the major parameters which play important roles in modelling the cure process may be identified as the temperature, the degree of cure of the resin, the resin viscosity, the resin flow velocity, the thickness of the processing material and the material properties, such as density, heat conductivity, etc. Most parameters are varied with respect to the time and spatial location.

To focus on the optimization aspects of study, several assumptions which simplify the formulation of the cure process are introduced. One

is that the temperature and the degree of cure of the composite material are uniformly distributed in a plane parallel to the tool plates. As a result, the parameters of the problem are functions of the time and the position along the thickness of the composite only. Secondly, the resin content in the material is assumed to be low so that only a small amount of resin will be squeezed out of the material. Consequently, the resin flow model as well as the pressure cycle can be neglected from considerations. Furthermore, the material properties which depend on the fiber-resin ratios can be assumed to be constant as well. Finally, it is assumed that there is no deviation between the cure temperature and the temperature on the surfaces of the material adjacent to the tool plates. Thus, the cure temperature can be considered as the boundary temperature of the material. The temperature distribution and the degree of cure are the only two state variables which are governed by a diffusion-reaction system. After simplification, the diffusion-reaction system can be used to describe the cure process of a continuous fiber composite with low resin content [8], and the cure process of a composite with the chopped fibers [2]. The interest of this study, however, is in compression molding of a filled polyester resin reinforced by chopped glass fibers. The unmolded composite is produced in sheets which are from 3 to 6 mm thick, typically. The resin consists of a thick dough and the chopped fibers (about 25 mm long) which are randomly oriented in the plane of the sheet. In this form, the material is called sheet molding compound, or simply SMC.

2.1 Diffusion-Reaction System

A diffusion-reaction system consists of an one-dimensional unsteady heat-conduction equation with its boundary and initial conditions, and a kinetic model of the cure rate of the resin. By using the finite element method and a numerical integrator, a computational algorithm is developed to analyze the thermo-chemical reaction. The numerical results of several examples are obtained by the developed scheme and compared with the existing solutions.

The temperature distribution $T(z,t)$ and the degree of cure $\alpha(z,t)$ of the resin inside the composite depend on the rate which heat is transmitted from the environment into the material. The temperature inside the composite can be calculated by using the law of conservation of energy together with an appropriate expression for the cure kinetics. By neglecting energy transferred by convection, the energy equation may be expressed as

$$\rho c\dot{T} = kT'' + \rho Hr\dot{\alpha} \tag{2.1}$$

with the boundary conditions,

$$T'(0,t) = 0, \qquad 0<t<\tau, \tag{2.2.a}$$

$$T(h,t) = T_c(t) \qquad 0<t<\tau, \tag{2.2.b}$$

and the initial condition,

$$T(z,0) = T_0(z), \qquad 0<z<h \tag{2.3}$$

where ρ and c are the density and the specific heat of the composite material, respectively, k is the thermal conductivity in the direction perpendicular to the plane of composite material, and $2h$ is the total

thickness. The temperature and the total or ultimate heat of reaction during the cure process are denoted by T and Hr, respectively. Moreover, the dot "•" on the top of a symbol indicates the time derivative and the superscript "′" denotes the spatial derivative. According to the assumptions discussed previously, all coefficients in Eqs. (2.1) - (2.3) are treated as constants. Note that the cure temperature $T_c(t)$ appears in the equation of the boundary condition Eqs. (2.2); and the last term in Eq. (2.1), $\rho Hr\dot{\alpha}$, is the rate of heat generated by the chemical reaction characterized by the state of cure α.

The state of cure depends strongly on the resin temperature. An empirical expression is usually employed to address the relation between the state of cure and the resin temperature. The degree of cure is defined as

$$\alpha = H(t)/Hr \tag{2.4}$$

where H(t) is the heat evolved from the beginning of the chemical reaction of resin to some intermediate time t. Both H(t) and Hr in Eq. (2.4) can be measured experimentally by, as an example; Differential Scanning Calorimetry (DSC). For an uncured material, α approaches to zero, and for a completely cured material, α approaches to one. For example, the cure rate equation of a stepwise isothermal cure process, can be defined for a polyester as follows

$$\begin{aligned}\dot{\alpha} &= f(\alpha,T) \\ &= (K_1 + K_2\alpha^m)(1 - \alpha)^n \\ &= (a_1 e^{-d1/RT} + a_2 e^{-d2/RT}\,\alpha^m)(1 - \alpha)^n \end{aligned} \tag{2.5}$$

where a_1, a_2, d_1, d_2, m, and n are constants, R is the universal gas constant, and K_1 and K_2 are exponential functions of the temperature. This example is taken from the research of compression molding conducted at the General Motors Research Laboratory [2].

Some observations of interest are stated as follows:

1. The state equations of the cure process are coupled with two state variables, namely, the temperature distribution $T(z,t)$ and the degree of cure $\alpha(z,t)$.
2. The non-homogeneous boundary value, $T_c(t)$, is to be considered as the design variable.

By using the following replacement of the temperature $T(z,t)$ as

$$T(z,t) = \bar{T}(z,t) + T_c(t), \tag{2.6}$$

the heat-conduction problem stated in Eqs. (2.1) - (2.3) can be simplified as an equation of $\bar{T}(z,t)$

$$\rho c\dot{\bar{T}} = k\bar{T}'' - \rho c\dot{T}_c + \rho H r f(\alpha,\bar{T},T_c), \tag{2.7.a}$$

with the homogeneous boundary conditions,

$$\bar{T}'(0,t) = 0, \qquad 0<t<\tau, \tag{2.7.b}$$

$$\bar{T}(h,t) = 0, \qquad 0<t<\tau, \tag{2.7.c}$$

and the initial condition,

$$\bar{T}(z,0) = T_o(z) - T_c(0), \qquad 0<z<h \tag{2.7.d}$$

where f is defined in Eq. (2.5). From here on $\bar{T}$ is abbreviated as T for further simplification. Because the initial temperature $T_o(z)$ is the

same as the initial cure temperature for most applications, the Eqs. (2.7) may have a homogeneous initial condition as well. Note also that the cure kinetics of the polyester are expressed in terms of the absolute temperature. Thus, the Kelvin's degree is used in this study as the unit of temperature.

2.2 Finite Element Model

The finite element discretization is introduced herein to convert the initial-boundary value problem, Eqs. (2.5) and (2.7), into a set of first order differential equations. These equations are then solved simultaneously by a numerical integration code called DE [7].

The quadratic and linear polynomials are used to interpolate the states of the temperature and the degree of cure, respectively. The notations T_{2i-1}, T_{2i}, and α_i denote the temperature, the temperature gradient and the degree of cure, respectively, at node i as shown in Fig. 2.1.

There are two degrees of freedom assigned at each node to approximate the temperature distribution. The interpolation functions of the temperature in each element are then defined as follows

$$
\begin{aligned}
N_1(z) &= 1 - 3\, z^2/\ell^2 + 2\, z^3/\ell^3 \\
N_2(z) &= -z + 2\, z^2/\ell - z^3/\ell^2 \\
N_3(z) &= 3\, z^2/\ell^2 - 2\, z^3/\ell^3 \\
N_4(z) &= z^2/\ell - z^3/\ell^2
\end{aligned}
\tag{2.8}
$$

where the notation of ℓ is the length of an element. Hence the temperature within an element is then given as

$$T(z,t) = \{N_1(z),\ N_2(z),\ N_3(z),\ N_4(z)\} \begin{Bmatrix} T_1(t) \\ T_2(t) \\ T_3(t) \\ T_4(t) \end{Bmatrix}$$

$$= \underline{N}^T \underline{T}. \tag{2.9}$$

As for the degree of cure, each node has one degree of freedom. The interpolation functions are defined as

$$L_1(z) = 1 - z/\ell$$
$$L_2(z) = z/\ell \tag{2.10}$$

where ℓ is the length of an element. Hence, the degree of cure within an element is defined as

$$\alpha(z,t) = \{L_1(z),\ L_2(z)\} \begin{Bmatrix} \alpha 1(t) \\ \alpha_2(t) \end{Bmatrix}$$

$$= \underline{L}^T \underline{\alpha} \tag{2.11}$$

Note that the shape functions employed here for the temperature distribution and the state of cure are the same as those for an elastic beam and a truss, respectively.

Equations (2.7.a) and (2.5) provide integral identities for any arbitrary testing functions u(z) and v(z):

$$0 = \int_0^h (\rho c\dot{T} - kT'' + \rho c\dot{T}_c - \rho Hrf)\, u\, dz$$

$$= \int_0^h (\rho c\dot{T}u + kT'u' + \rho c\dot{T}_c u - \rho Hrfu)\, dz - kT'u\Big|_0^h$$

$$= \sum_1^{NE} \int_{z_i}^{z_{i+1}} (\rho c\dot{T}u + kT'u' + \rho c\dot{T}_c u - \rho Hrfu)\, dz \qquad (2.12)$$

and

$$0 = \int_0^h (\dot{\alpha} - f)\, v\, dz$$

$$= \sum_1^{NE} \int_{z_i}^{z_{i+1}} (\dot{\alpha} - f)\, v\, dz \qquad (2.13)$$

Where the testing function $u(z)$ has to satisfy the kinematic boundary condition, Eq. (2.7.c) and NE denotes the number of elements. The boundary terms of Eq. (2.12) drop because of $u(h) = 0$, and $T'(0,t) = 0$. The last equality in Eq. (2.13) indicates that the domain $(0<z<h)$ has been divided into NE finite elements. Considering any interpolation functions N_j and L_j defined previously as the testing functions $u(z)$, and $v(z)$, respectively, and using Eqs. (2.9) and (2.11), one can establish two matrix equations for the nodal temperature and the nodal degree of cure as

$$\rho c[C]\dot{\underline{T}} + k[K]\underline{T} + \rho c\underline{P}\dot{T}_c = \underline{Q}(\alpha,T,T_c), \qquad (2.14.a)$$

$$[M]\dot{\underline{\alpha}} = \underline{R}(\alpha,T,T_c) \qquad (2.14.b)$$

with the boundary conditions,

$$\underline{I} = \{0,\ T_2(o),\ T_3(o),\ \cdots,\ T_{2n-1}(o),\ 0\}^T \qquad (2.14.c)$$

where the unknowns are vectors $\underline{I} = \{T_1, T_2, \cdots, T_{2n}\}^T$ and $\underline{\alpha} = \{\alpha_1, \alpha_2, \ldots, \alpha_n\}^T$ for n = NE + 1 as the total number of nodes. Note that $T_1(t)$ and $T_{2n}(t)$ are always zeros in the analysis according to the boundary conditions, $T(h,t) = 0$ and $T'(0,t) = 0$, respectively. The initial conditions for each of the components in $\underline{I}$ and $\underline{\alpha}$ are

$$T_{2i-1}(0) = T_{Room} - T_c(0),$$

$$T_{2i}(0) = 0,$$

and

$$\alpha_i(0) = 0$$

where i is the nodal number, and T_{2i-1} and T_{2i} are corresponding to the temperature and the temperature gradient at the node i. Moreover, T_{Room} represents the temperature of the composite at the onset of the cure process that is usually uniformly distributed. The detailed derivation of the matrix equations, Eq. (2.14), is given in Appendix A. The above equations, coupled with each other through the non-linear terms on the right side of Eq. (2.14), can be solved simultaneously by using a computer code called DE.

The DE program is one of predictor-corrector integration algorithms using Adams family of formulas. The truncation error is controlled by varying both the step size and the order of the polynomial approximation. The truncation error of the solution Z_{n+1} at time step t_{n+1} is required by the DE program to satisfy the following relation:

$$|\text{trunc}| \leq \text{ABSERR} + \text{RELERR} \cdot |Z_n|$$

where Z_n is the solution of the differential equation at t_n, and the values ABSERR and RELERR are supplied by the user.

The DE program is quite easy to be used and has the capability to manage moderate stiff equations which happen commonly in the problems of chemical kinetics. To maintain a unified accuracy in the analysis, the computation of two state variables, namely, the temperature and the degree of cure, are subjected to the same error tolerance in this study.

2.3 Numerical Examples

In this section, three examples have been studied. The numerical results are in a very good agreement with the theoretical solution in example one, and with the numerical solution reported in the literature [2,8,9,10] in example two and three.

Example 1: one-dimensional heat conduction with prescribed end temperature.

This problem can be described by the following equation,

$$\rho c\dot{T} = kT'' \tag{2.15}$$

with the boundary conditions,

$$T'(0,t) = 0, \qquad 0 \leq t \leq \tau,$$

$$T(h,t) = 0, \qquad 0 \leq t \leq \tau,$$

and the initial condition,

$$T(z,0) = T_o, \qquad 0 \leq z \leq h.$$

The exact solution of this problem [9] is given as

$$T(z,t) = \sum_{n=1,3,5\ldots}^{\infty} \frac{4T_o}{n\pi} \operatorname{Sin} \frac{n\pi z}{\ell} e^{-(n^2\pi^2 kt/\rho c\ell^2)} \tag{2.16}$$

where the notation ℓ is the total thickness 2h.

The finite element problem is solved with $\ell = 10$, $k = 1$, $\rho c = 1$, and $T_o = 100$. Twenty equal-spaced elements are used. Both the finite element and the exact solution are shown in Fig. 2.2 for the time grids $t = 4.0, 8.0, 12.0, 16.0, 20.0$, respectively. Note that a very good agreement exists between the finite element solution and the exact solution.

Example 2: one-dimensional heat conduction problem coupled with a given chemical-kinetic model [2].

This example simulates the compression modelling of composite laminates with its thickness 10 mm. The initial (material) temperature is 298°K and the cure temperature is taken as a constant temperature, i.e., $T_c(t) = 423°K$. This problem is described by Eqs. (2.1) - (2.3). The coefficients of this problem are given in Table 2.1.

Using the finite element method to solve this problem, sixteen elements are used. The finite element results of the temperature distribution and the degree of cure compared with the results of the General Motor Research report [2] are given in Fig. 2.3 and Fig. 2.4, respectively. Solid curves are from the General Motor Research report; the dash lines are calculated by Eq. (2.14). This example also shows a good agreement between the calculated data and that of the General Motor Research report.

Example 3: one-dimensional heat conduction problem coupled with a given-kinetic model of thick-section autoclave cured composites [8,10].

One simulates the autoclave processing of 192 ply prepregs with 32% Hercules resin content. The resin flow can be neglected in this example, because the resin content is low. To focus on the heat conduction and the chemical-kinetic models, the measured temperature on

the surface of the composite laminate is used as the boundary temperature, instead of the temperature of the cure cycle. Although the heat flux, induced by the heat convection of autoclave air temperature, is neglected, the numerical result is in excellent agreement with Loos' data [10], as shown in Fig. 2.5.

CHAPTER III

THERMAL DESIGN SENSITIVITY ANALYSIS

The derivatives of functionals of responses with respect to the design variables are often referred to as design sensitivity derivatives. Most general optimization algorithms require such derivatives which can be used to approximate constraints and to choose a search direction to obtain a set of improved design variables. It is then needed to have a reliable means to calculate the design sensitivity derivatives.

Two commonly used methods for design sensitivity analysis, namely, the adjoint variable method and the direct differentiation method, are studied in this chapter. The comparisons of numerical results obtained by these two methods demonstrate that the direct differentiation method is a better choice for this study.

3.1 Techniques of Thermal Design Sensitivity Analysis

As discussed previously, the cure uniformity and completeness for the cure cycle design. However, it is difficult to cast the measurement of the cure uniformity and completeness in a precisely mathematical form. To focus on the study of thermal design sensitivity analysis in this section, the cure uniformity is simply represented by the least-squared integral of the deviation between the pointwise temperature and the averaged temperature as

$$\psi_o = \int_0^\tau \left[\int_0^h T^2\, dz - \left(\int_0^h T\, dz\right)^2/h\right] dt. \qquad (3.1)$$

The above functional defines a global sense of temperature uniformity across the thickness of the composite during the cure process. It is expected that the temperature uniformity yields the cure uniformity. Other mathematical expressions of the cure uniformity are to be discussed in the following chapter of optimal cure cycle design. On the other hand, the following pointwise inequality may be used to force the cure reaction to be completed at the end of the cure process.

$$\alpha(z,\tau) \geq \alpha_f, \qquad 0 \leq z \leq h \qquad (3.2)$$

where τ is the total time interval of the cure process and α_f is a constant assigned to indicate the completeness of the degree of cure. The numerical techniques to calculate the design derivatives of the functional ψ_o and the state variable α, $\frac{d\psi_o}{db}$ and $\frac{d\alpha}{db}$, are to be addressed hereafter. Note that the design variable b is a parameter associated with the cure temperature profile.

In general, there are four ways to calculate the thermal design derivatives, namely, the finite difference method, the Greene's function approach, the direct differentiation method (the behavior space approach), and the adjoint variable method (the dummy load method). The last two methods are often mentioned in the literature [3,4,11,12]. Both methods lead to a set of linear equations that have a similar structure to the original system.

The computational efforts regarding the direct differentiation method and the adjoint variable method depend mainly on the numbers of constraints and design variables of concern. The direct differentiation

method requires the solution of a differential equation for each design variable, while the adjoint variable method requires the solution of an adjoint equation for each constraint. Consequently, the direct differentiation method is more efficient to calculate the design derivatives than the adjoint variable method when the number of design variables is smaller than the number of constraints, or vice versa.

It is also known that the direct differentiation method provides equations of design derivatives which have exactly the same differential operator as that of the original equations. The equations of design derivatives can, therefore, be solved simultaneously with the original system equations subjected to the same numerical error tolerance. Furthermore, without extra efforts, the results of the direct differentiation approach provide the histories of design derivatives of functionals and state variables. This information is very useful for a designer to reconstruct the design space. One may check this information to see whether a design variable of concern attributes to the perturbation of the functional of concern consistently over a long or just a limited period of time.

3.2 The Adjoint Variable Method

The problem of interest is to derive a set of equations for computing the design sensitivities of a functional and the state variables. The variation of a function ψ with respect to a design variable b is defined as

$$\delta\psi = \lim_{\varepsilon \to 0} \frac{\psi(t,b+\varepsilon\delta b) - \psi(t,b)}{d\varepsilon}$$

$$= \left. \frac{d\psi\ (t,b+\varepsilon\delta b)}{d\varepsilon} \right|_{\varepsilon=0}$$

$$= \psi' \delta b \tag{3.3}$$

where δb is the perturbation of design variable and ψ' is defined as $\frac{d\psi}{db}$. The variations of state variables can be defined by a similar fashion. Using the functional defined in Eq. (3.1) as an example, the variation of this functional is then given as

$$\delta\psi = \int_0^\tau \left[\int_0^h 2T - \frac{2}{h}\int_0^h T\, dz\right] \delta T\, dz\, dt. \tag{3.4}$$

The governing equations of the diffusion-reaction system defined in Eqs. (2.5) and (2.7) are

$$\rho c\dot{T} = kT'' - \rho c\dot{T}_c + \rho H r f(\alpha,T,T_c),$$

$$\dot{\alpha} = f(\alpha,T,T_c).$$

For arbitrary functions $\lambda(z,t)$ and $s(z,t)$ it is evident that

$$0 = \int_0^\tau \int_0^h \lambda(\rho c\dot{T} + \rho c\dot{T}_c - kT'' - \rho H r f)\, dz\, dt, \tag{3.5}$$

and

$$0 = \int_0^\tau \int_0^h S(\dot{\alpha} - f)\, dz\, dt. \tag{3.6}$$

The variations of these equations yield

$$0 = \int_0^\tau \int_0^h (\rho c \delta \dot{T} \lambda + \rho c \delta \dot{T}_c \lambda - \rho \delta T'' \lambda - \rho Hr \frac{\partial f}{\partial \alpha} \delta \alpha \lambda$$

$$- \rho Hr \frac{\partial f}{\partial T} \delta T \lambda - \rho Hr \frac{\partial f}{\partial T_c} \delta T_c \lambda) \, dz \, dt, \tag{3.7}$$

and

$$0 = \int_0^\tau \int_0^h (S \delta \dot{\alpha} - S \frac{\partial f}{\partial \alpha} \delta \alpha - S \frac{\partial f}{\partial T} \delta T - S \frac{\partial f}{\partial T_c} \delta T_c) \, dz \, dt. \tag{3.8}$$

Integrating by parts, the above equations can be rewritten as

$$0 = \int_0^\tau \int_0^h [(-\rho c \dot{\lambda} - k \lambda'' - \rho Hr \lambda \frac{\partial f}{\partial T}) \delta T + (-\rho c \dot{\lambda} - \rho Hr \lambda \frac{\partial f}{\partial T_c}) \delta T_c$$

$$- \rho Hr \lambda \frac{\partial f}{\partial \alpha} \delta \alpha] \, dz \, dt + \int_0^\tau k \lambda' \delta T \Big|_0^h dt$$

$$- \int_0^\tau k \lambda \delta T' \Big|_0^h dt + \int_0^h \rho c \lambda \delta T \Big|_0^\tau dz + \int_0^h \rho c \lambda \delta T_c \Big|_0^\tau dz, \tag{3.9}$$

and

$$0 = \int_0^\tau \int_0^h (-\dot{S} \delta \alpha - S \frac{\partial f}{\partial \alpha} \delta \alpha - S \frac{\partial f}{\partial T} \delta T - S \frac{\partial f}{\partial T_c} \delta T_c) \, dz \, dt$$

$$+ \int_0^h S \, \delta \alpha \Big|_0^\tau dz. \tag{3.10}$$

Adding Eqs. (3.4), (3.9), and (3.10) up, one has the variation of the functional ψ as

$$\delta\psi = \int_0^\tau \int_0^h \left[(2T - \frac{2}{h}\int_0^h T dz) - \rho c\dot{\lambda} - k\lambda'' - \rho Hr \frac{\partial f}{\partial T} - S\frac{\partial f}{\partial T}\right]\delta T \, dz \, dt$$

$$+ \int_0^\tau \int_0^h (-\rho Hr\lambda \frac{\partial f}{\partial \alpha} - \dot{S} - S\frac{\partial f}{\partial \alpha})\, \delta\alpha \, dz \, dt$$

$$+ \int_0^\tau \int_0^h (-\rho c\dot{\lambda} - \rho Hr\lambda \frac{\partial f}{\partial T_c} - S\frac{\partial f}{\partial T_c})\, \delta T_c \, dz \, dt$$

$$+ \int_0^h \rho c\lambda \delta T_c \Big|_0^\tau dz + \int_0^\tau k\lambda' \delta T \Big|_0^h dt - \int_0^\tau k\lambda \delta T' \Big|_0^h dt$$

$$+ \int_0^h \rho c\lambda \delta T_c \Big|_0^\tau dz + \int_0^h S\, \delta\alpha \Big|_0^\tau dz. \qquad (3.11)$$

Note that $\lambda(z,t)$ and $s(z,t)$ are arbitrary functions, and the only two unknowns in the above equation are the design derivatives δT and $\delta\alpha$. One may now specify the variables λ and s in such a way that all terms associated with δT and $\delta\alpha$ are dropped. This can be accomplished by introducing the following adjoint equations for λ and s:

$$0 = \rho c\dot{\lambda} + k\lambda'' + \rho Hr \frac{\partial f}{\partial T} + S\frac{\partial f}{\partial T} - (2T - \frac{2}{h}\int_0^h T dz), \qquad (3.12)$$

and

$$0 = \dot{S} + \rho Hr\lambda \frac{\partial f}{\partial \alpha} + S\frac{\partial f}{\partial \alpha} \qquad (3.13)$$

with the terminal conditions,

$$\lambda(z,\tau) = 0, \qquad 0<z<h, \qquad (3.14)$$

$$s(z,\tau) = 0, \qquad 0<z<h, \tag{3.15}$$

and the boundary conditions,

$$\lambda'(0,t) = 0, \qquad 0<t<\tau, \tag{3.16}$$

$$\lambda(h,t) = 0, \qquad 0<t<\tau, \tag{3.17}$$

Then, the combination of Eqs. (3.11) - (3.17) provides a simple formula for the design derivative of the functional,

$$\delta\psi = \int_0^\tau \int_0^h \left(-\rho c\dot{\lambda} - \rho Hr \frac{\partial f}{\partial T_c} - S \frac{\partial f}{\partial T_c}\right) \delta T_c \, dz \, dt$$

$$+ \int_0^h \rho c\lambda(o) \, \delta T_c(o) \, dz \, . \tag{3.18}$$

Equation (3.18) shows that the design derivative of ψ, namely, $\delta\psi$, is a functional of state variables α and T, and the adjoint variables λ and s. The α and T can be solved by the finite element method as discussed in Chapter 2 and Appendix A. The matrix equations which solve the nodal values of $\underline{\alpha}$ and $\underline{T}$ are mentioned in Eq. (2.14). Since the adjoint variables of Eqs. (3.12) - (3.13) form an "adjoint" diffusion-reaction system similar to the original one, the same numerical scheme used to solve the state variables α and T can be extended here to compute the adjoint variables s and λ. For instance, using the shape functions of α and T in Eqs. (2.9) and (2.11) to interpolate the adjoint variables λ and s obtains the following matrix equations for nodal values of λ and s.

$$\rho c[C] \, \dot{\underline{\lambda}} = k[K]\underline{\lambda} - \underline{Q}^* + 2 \, \underline{T}^T \, [C] - \frac{2}{h} \, \underline{T}^T \, \underline{P} \, \underline{P}^T, \tag{3.19}$$

$$[M]\,\dot{\underline{S}} = \underline{R}^{*} \tag{3.20}$$

with proper boundary and terminal conditions. The $\underline{Q}^{*}$ and $\underline{R}^{*}$ in the above equations have definitions similar to their counterparts of Eqs. (A.17) and (A.18) defined in Appendix A.

In general, the adjoint equations can not be solved simultaneously with the original system equations. Because of the terminal conditions, the adjoint equations can be solved by either the backward integration along the real time t - axis directly or the forward integration along the artificial time t^{*} - axis, provided that the independent variable t is changed to t^{*} as $t^{*} = \tau - t$. However, both approaches require the solutions of the original system equations prior to solving the adjoint equations.

3.3 The Direct Differentiation Method

The direct differentiation method is an approach that takes derivatives of differential equations with respect to a single design variable directly.

For a given functional, Eq. (3.1), and the governing equations of the diffusion-reaction system, Eqs. (2.5) and (2.7), the direct differentiation results in the following equations in terms of design derivatives $\frac{dT}{db}$ and $\frac{d\alpha}{db}$ as:

$$\psi' = \int_{0}^{\tau} \left[\int_{0}^{h} 2T \frac{dT}{db}\, dz - \frac{2}{h} \left(\int_{0}^{h} T dz \right) \left(\int_{0}^{h} \frac{dT}{db}\, dz \right) \right] dt, \tag{3.21}$$

$$\rho c \frac{d\dot{T}}{db} = k \frac{dT''}{db} - \rho c \frac{d\dot{T}_c}{db} + \rho Hr \frac{\partial f}{\partial \alpha} \frac{d\alpha}{db} + \rho Hr \frac{\partial f}{\partial T} \frac{dT}{db}$$

$$+ \rho Hr \frac{\partial f}{\partial T_c} \frac{dT_c}{db}, \tag{3.22}$$

and

$$\frac{d\dot{\alpha}}{db} = \frac{\partial f}{\partial \alpha} \frac{d\alpha}{db} + \frac{\partial f}{\partial T} \frac{dT}{db} + \frac{\partial f}{\partial T_c} \frac{dT_c}{db}. \tag{3.23}$$

It is assumed that $T(z,b,t)$ and $\alpha(z,b,t)$ have enough regularity in the time-spatial domain and in the design space. Thus, the order of the differentiation is exchangeable, i.e.,

$$\frac{d\dot{T}}{db} = \frac{dT_b}{dt},$$

$$\frac{d\dot{\alpha}}{db} = \frac{d\alpha_b}{dt},$$

and

$$\frac{dT''}{db} = T_b''$$

where the subscript "b" denotes the design derivative.

Based on the same finite element discretization as used in solving the original diffusion-reaction system discussed in Chapter 2, Eqs. (3.21) - (3.23) can be converted into a set of matrix equations

$$\psi_b = \int_o^\tau (2\underline{T}^T [C] \underline{T}_b - \frac{2}{h} \underline{I}^T \underline{P} \underline{P}^T \underline{T}_b)\, dt, \tag{3.24}$$

$$\rho c[C] \dot{\underline{T}}_b = - k[K] \underline{T}_b - \rho c \underline{P} \frac{d\dot{T}_c}{db} + \underline{\bar{Q}}, \tag{3.25}$$

and

$$[M] \dot{\underline{\alpha}}_b = \underline{\bar{R}} \tag{3.26}$$

The construction of the above equations are discussed in Appendix B.

Note that the coefficient matrices of $\dot{\underline{T}}_b$ and $\dot{\underline{\alpha}}_b$ in Eqs. (3.25) and (3.26) are identical to those of $\underline{T}$ and $\underline{\alpha}$ defined in Eqs. (2.14). Therefore, the same numerical scheme and numerical tolerance can be applied to solve both Eqs. (2.14), (3.25) and (3.26) simultaneously for state variables, $\underline{T}$ and $\underline{\alpha}$, and design derivatives, $\underline{T}_b$ and $\underline{\alpha}_b$. In this way, the state variables and the design derivatives achieve the same numerical accuracy, though an additional set of equations such as Eqs. (3.25) and (3.26) is needed in this approach for each design variable b.

Regarding the computational efficiency, it is worthwhile mentioning two notes here:

1. Because the coefficient matrices of $\dot{\underline{T}}_b$ and $\dot{\underline{\alpha}}_b$ are identical to those of $\dot{\underline{T}}$ and $\dot{\underline{\alpha}}$, the triangular factorizations of matrices [C] and [M] are needed to be done only once. The calculation of $\dot{\underline{T}}_b$ and $\dot{\underline{\alpha}}_b$ can be carried out by back substitution for each of the design variables.
2. Compared to the original system equations, the right side of equations for computing $\underline{T}_b$ and $\underline{\alpha}_b$, such as Eqs. (3.25) and (3.26), may have different frequency contents. Thus, to maintain the sa e numerical accuracy, a smaller time step Δt may be required for the DE program to solve the pairs $(T, \underline{\alpha})$ and $(\underline{T}_b, \underline{\alpha}_b)$ simultaneously.

Once $\underline{T}$ and $\underline{T}_b$ are available, the design derivative given in Eq. (3.24) can be easily obtained by the numerical integration. Another suggestion is to rewrite the integral form of Eq. (3.24) as a differential equation of ψ given as

$$\dot{\phi}_b = 2\,\underline{T}^T\,[C]\,\underline{T}_b - \frac{2}{h}\,\underline{T}^T\,\underline{P}\,\underline{P}^T\,\underline{T}_b. \qquad (3.27)$$

The above equation of ϕ_b can then be solved simultaneously with equations of $(\underline{T}, \underline{\alpha})$ and $(\underline{T}_b, \underline{\alpha}_b)$. In this way, one extra design derivative ϕ_b for each design variable is introduced in the design sensitivity analysis. However, the accuracy of ϕ_b is secured. Equation (3.27) is used in the next section and Chapter 4 to compute the ϕ_b.

3.4 Numerical Examples

Two examples which deal with the cure process of compression molding are presented in this section to discuss the numerical accuracy of the adjoint variable method and the direct differentiation method for calculating the thermal design derivatives. The accuracy of the thermal design sensitivity analysis can be checked by using the fundamental definition of design derivatives which can be approximated by the finite difference. In other words, it is mathematically true for a small perturbation of design variable Δb that

$$\phi' \equiv \frac{d\phi}{db}$$

$$\cong \frac{\Delta\phi}{\Delta b}.$$

The finite perturbation of the design variable Δb is defined as the difference between a perturbed design b^* and the nominal design b, i.e., $\Delta b = b^* - b$. As a result, it follows that

$$\Delta\phi = \phi(b^*) - \phi(b)$$

$$\cong \phi'\,\Delta b. \qquad (3.28)$$

The above equation provides a simple means to check the accuracy of the design sensitivity analysis. Nevertheless, the difficulty of this method is the selection of Δb. If Δb is too large, the approximation in Eq. (3.28) is not valid. On the other hand, if Δb is too small, the round-off error in the computation of $[\psi(b^*) - \psi(b)]$ becomes too large to apply the approximation of Eq. (3.28) for the sensitivity calculation. In the following examples, several values of Δb are used to check the accuracy of the design sensitivity analysis in order to ensure the quality of the approximation given in Eq. (3.28).

The first example presented here deals with the cure process Eqs. (2.14) in which the cure temperature of the process is assumed to be a constant temperature. The nominal cure temperature is taken as 423°K. According to the approximation defined in Eq. (3.28), the results shown in Fig. 3.1 demonstrate that the thermal design sensitivity calculated by the direct differentiation method is more accurate than the results calculated by the adjoint variable method. Moreover, by using the direct differentiation method, one can also get the time histories of the design derivatives of state variables as shown in Figs. 3.2 and 3.3.

The second example deals with the same cure process as example one. However, the profile of the cure temperature is assumed to be the same as the one given in Fig. 3.4 where the heating rate is considered as a design variable. The nominal value of the heating rate is taken as 4.0°K/sec. The results of thermal design sensitivity analyses are shown in Fig. 3.5. The time histories of the design derivatives are shown in Figs. 3.6 and 3.7.

From the above two examples, it is obvious that the direct differentiation method provides more accurate results than the adjoint variable method does. The direct differentiation method also yields the time histories of the design derivatives. In addition, the information of design derivatives of the pointwise constraints can be obtained by using the direct differentiation method without extra cost.

Based on the numerical study, it is concluded that the direct differentiation method is superior to the adjoint variable technique in terms of accuracy and physical interpretation of results. In the next chapter, the thermal design sensitivity is to be calculated by using the direct differentiation method.

CHAPTER IV

OPTIMAL CURE CYCLE DESIGN

At the present time, the cure cycle is generally selected by the method of parametric study conducted by either physical experiments or numerical simulation [1]. This "trial and error" type of approach may be costly and inefficient. Therefore, the development of a unified and systematical approach to design the "best" cure cycle for a given composite material is needed.

The optimal design of cure cycles studied here are to find the optimal cure temperature during the cure process to have the thermosetting resin cured as uniformly as possible and to assume the resin completely cured at the end of the cure process.

Numerical results presented in this chapter have been obtained by a recursive quadratic programming algorithm with an active set strategy, called a linearization method [13]. The main reason to use this linearization method is that it has been proved to be globally convergent. The linearization method, with its active set strategy, minimizes the number of constraints which must be considered in each design iteration. The detailed derivation of this algorithm can be found in reference [13,14]. The concept of this algorithm is that, rather than directly solving the optimal criteria, a small perturbation for each design variable is determined in each iteration to reduce the objective function and correct the violation. Note that, in this

approach, the reduction of the objective function and the correction of the constraint violations are approximated by the design gradients. In general, whenever, the objective function can not be reduced further by changing the design variables and all constraints are satisfied, it is indicated that the linearization method is converged and the optimal solution is obtained. In this algorithm, however, it has been proved [15] that a local optimal solution is found when the ℓ^2 norm of the perturbation of design variables approaches to zero. The complete flow chart of this algorithm is listed in Fig. 4.1. As shown in the figure, the proposed CAD method consists of three uncoupled modules: namely, optimization, analysis, and sensitivity calculation. Once the analysis capability of any cure process is established, the optimization and sensitivity calculation modules can be added onto it to constitute a unified CAD method and to generate an optimal cure cycle systematically. In this thesis a well documented DE program is used for the numerical integration of state equations and equations of thermal design derivatives.

4.1 Problem Statement

As mentioned, optimal design techniques have been successfully applied to various transient problems. In general, an optimal design problem consists of design variables, the objective, constraint functions, and state equations which describe the physical model of interest.

In our study, the process of interest is a compression molding of a filled polyester resin reinforced by chopped glass fibers SMC [2]. The state equations are limited to a heat conduction equation and an

empirical equation which addresses the chemical-kinetic reaction of resin.

Since this study excludes the resin flow and the effects of the pressure cycle, the selection of the cure temperature is then limited to the following considerations:

a) The maximum temperature inside the composite during the cure process can not exceed a value of 500°K in this study.

b) At the end of the cure process, the material is cured completely. Mathematically, the degree of cure is required to be at least 0.85 when the cure process is completed.

c) The material is cured uniformly at any time during the cure process.

The first two requirements may be formulated as constraints

$$\psi_1 : T(t) \leq 500\ ^\circ K, \qquad 0 \leq t \leq \tau, \tag{4.1}$$

$$\psi_2 : \alpha(\tau) \geq 0.85 \tag{4.2}$$

where τ is the operational period of the cure process. The τ is not considered as a design variable in this study. The last requirement can be met by formulating it as the objective function of the optimal design. Since the degree of cure is a function of temperature, the uniform distribution of temperature across the thickness of the material implies the cure uniformity. The objective of the optimal design may then be set to achieve the temperature uniformity across the section of the material during the cure process. The objective function ψ_o is then defined as the greatest value of the standard derivation of temperature distribution which happens during the cure process

$$\psi_o(T_c,t) = \underset{0\leq t\leq\tau}{\text{Maximum}} \left[\int_o^h T^2 dz - \left(\int_o^h T dz\right)^2/h\right]. \qquad (4.3)$$

The minimum of the objective function, $\psi_o(T_c,t) = 0$, corresponds to a uniform temperature distribution inside the composite at any time during the cure process. Consequently, a uniform cure state can be accomplished during the complete duration of the cure process.

To sum up, the optimal cure cycle design is defined as follows:

"The optimal cure temperature (temperature profile) is designed, subject to the limitations regarding the maximum temperature and the state of cure, so as to achieve a uniform temperature distribution along the cross section of the material at any time during the cure process."

The mathematical formulation of the stated optimal design problem is a mimimax problem given as

$$\underset{T_c(t)}{\text{Minimize}} \ \underset{0\leq t\leq\tau}{\text{Maximum}} \ \left[\int_o^h T^2 dz - \left(\int_o^h T dz\right)^2/h\right]$$

subject to the constraints stated in Eqs. (4.1) - (4.2) where the temperature $T(t)$ and the degree of cure $\alpha(t)$ are the solutions of state equations.

It is known that the objective function of a minimax problem is discontinuous in the design space [16]. To avoid the computational difficulty, one may modify the optimal design problem to a standard form by introducing an extra design variable b and an additional constraint ψ_3 as

$$\underset{T_c(t),\ b}{\text{Minimize}} \quad \psi_o = b$$

subject to

$$\psi_1 : T(t) \leq 500\ ^\circ K, \qquad 0\leq t\leq\tau, \qquad (4.4)$$

$$\psi_2 : \alpha(\tau) \geq 0.85 \tag{4.5}$$

$$\psi_3 : [\int_o^h T^2 dz - (\int_o^h T dz)^2/h] \leq b, \qquad 0 \leq t \leq \tau. \tag{4.6}$$

The design function $T_c(t)$ can now be parametrized by a linear combination of design parameters and given functions such as

$$T_c(t) = \sum_1^{ND} b_i N_i^*(t)$$

where ND is the total number of design variables, b_i, and $N_i^*(t)$ are any independent functions. In this presentation, the design function is simply represented by a combination of linear polynomials and sinusoids

$$T_c(t) = T_o + b_1 t + b_2 \sin(\pi t/\tau) + b_3 \sin(2\pi t/\tau) +$$

$$b_4 \sin(3\pi t/\tau), \tag{4.7}$$

where T_o is the room temperature and b_1, b_2, b_3, and b_4 are to be determined by the optimal design algorithm. As a result, the design space becomes finite dimensional, and the design sensitivity (or gradient) of temperature T(t) and state of cure $\alpha(t)$ are taken as derivatives with respect to design parameters b_1, b_2, b_3, and b_4. For example, the design derivatives of constraint functions, Eqs. (4.4) - (4.6), can be derived as

$$\frac{\partial \psi_1}{\partial b_i} = \left(\frac{\partial T(t)}{\partial b_i}\right)/500, \tag{4.8}$$

$$\frac{\partial \psi_2}{\partial b_i} = \left(\frac{\partial \alpha(\tau)}{\partial b_i}\right)/0.85, \tag{4.9}$$

and

$$\frac{\partial \psi_3}{\partial b_i} = \frac{2}{b}\left[\int_o^h T \frac{\partial T}{\partial b_i}\, dz - \left(\int_o^h T dz\right)\left(\int_o^h \frac{\partial T}{\partial b_i}\, dz\right)/h\right]. \qquad (4.10)$$

It is obvious that the design sensitivities of $\frac{\partial T}{\partial b_i}$ and $\frac{\partial \alpha}{\partial b_i}$ are needed for the calculation of the above function gradients. Note that the pointwise constraints, ψ_1 and ψ_3, are imposed at every time grid point in this study. The optimal cure cycle $T_c(t)$ of the above problem can be found numerically by calculating the thermal sensitivity analysis and by using a gradient-based mathematical programming technique. As discussed in the last chapter, the direct differentiation method is employed hereafter to compute the required thermal design derivatives.

4.2 Numerical Examples

To show the applicability of the proposed CAD scheme for the optimal cure cycle design, four examples associated with various problem formulations are discussed and presented in this section.

Example 1.

The objective function ψ_o defined by Eq. (4.3) is minimized to find an optimal cure cycle design for processing a chopped glass fibers SMC with 10 mm in thickness. The total processing time is limited to 100 seconds. The maximum temperature allowed inside the SMC is 500°K; and the degree of cure α is required to reach at least 0.85 at the end of the cure process.

The physical and kinetic properties of the SMC material are given in Table 2.1 [2]. It requires 22 iterations of the algorithm to obtain the optimal solution for this case. Numerical results for the optimal

design are listed in Table 4.1. Figure 4.2 shows the cure temperatures computed at iterations 1, 11, and 22, respectively. It should be noted that the cure cycles designed in this example are always made to start from room temperature which is different from the common practice with pre-warmed press platens employed in the compression molding process. The initial cure temperature (iteration 1) has a peak and a valley at around 20 and 60 seconds, respectively. Among the iterations (1, 11, and 22) the initial heating rates are seen to decrease gradually; eventually a single peak near 70 seconds is obtained for the optimal solution. The values of the objective functions (ϕ_0 computed during iterations) are shown in Fig. 4.3. The optimal cure cycle indeed delivers a more uniformly distributed temperature. The optimal solution has reduced the maximal value of temperature deviation from 2,700 to 378 units.

Temperature distributions across the thickness of the SMC at selected instants of 20, 60, and 100 seconds during the cure process are compared for iterations 1, 11, and 22, shown in Fig. 4.4a, b, and c, respectively. As noted previously in Fig. 4.2, the low initial heating rate helps the optimal cure cycle (iteration 22) achieve a more uniform temperature distribution at the early 20 seconds into the cure process. At the 60 seconds into the cure process, the cure cycle of the eleventh iteration obtains a better distribution profile as seen in Fig. 4.4b. This is also a direct consequence of the negative heating rates (cooling) between 30 to 50 seconds observed from Fig. 4.2. On the other hand, the high initial heating rate provided by the cure cycle of iteration 1 has strongly triggered the kinetic reaction in the first 20 seconds into the cure process. Consequently, a highly non-uniform

temperature is observed between 30 to 50 seconds, even though the cure cycle of iteration 1 possesses the steepest cooling rate within the same time interval among all of the cure cycles shown in Fig. 4.4. In other words, the heat change caused by the steepest cooling rate needs enough time to be diffused into the material in order to offset the extra heat generated by chemical reactions between 30 to 50 seconds. It is, therefore, expected that, as shown in Fig. 4.4c, the more uniform temperature distribution can be achieved by the cure cycle of iteration 1 at the latter stage of the cure process.

The distributions of the states of cure α across the SMC thickness are shown in Figs. 4.5, 4.6, and 4.7 for the cure cycles of iterations 1, 11, and 22, respectively. In all cases, the cure of the resin starts from the surface regime and extends into the core of SMC. The cure cycle of iteration 1 requires the shortest time (60 seconds) to complete the cure reaction of the material with $\alpha > 0.85$.

The low cure temperatures provided by the optimal cure cycle at the intial 40 seconds into the cure process can hardly trigger the chemo-kinetic reactions of the resin matrix as seen from Fig. 4.7. However, for the optimal cure cycle, the rate of the cure process speeds up in the next 40 seconds and eventually the degree of cure exceeds the 0.85 limit throughout the SMC material at the end of the cure cycle.

Example 2.

This is identical to the problem stated in Example 1 except that the total processing time is extended to 150 seconds.

The optimal cure cycle of Example 1 is used as the initial trial cure cycle studied here. The algorithm needs another 25 iterations to reach the optimal solution for this problem. Table 4.2 lists the

numerical results for the optimal design. The optimal cure cycles of Examples 1 (iteration 1) and 2 (iteration 25) are compared in Fig. 4.8. It is noted that the cure cycle of Example 2 possesses even slower initial heating rates, and the cooling period is no longer needed over the entire cure cycle. The values of the objective functions are also compared in Fig. 4.9 as indicated by a drop of maximum temperature deviation from 250 to 110 units, the extension of the total processing time enables an optimally designed cure cycle to achieve better temperature uniformity during the cure process. Such improvement is also magnified in Fig. 4.10 where temperature distributions across the SMC thickness at selected instants during the cure process for the above two cure cycles are compared. The distribution of the state of cure for the optimal cure cycle of this example is shown in Fig. 4.11. The cure behavior basically shows the same characteristics as the optimal solution of Example 1.

Example 3.

This is identical to the problem stated in Example 1, except that the maximum cure state deviations defined by a new objective function (Eq. 4.11) is minimized; and the total processing time is extended to 150 seconds.

The goal of present cure cycle design is to have the thick composite SMC cured uniformly. It is rationalized that perfectly uniform temperature distribution across the SMC thickness all the time during the cure process will secure such an objective. However, as shown by the previous two examples, the optimal cure cycle of Example 2 does not establish significantly uniform states of cure, even though the temperature uniformity (as indicated by the objective functions ψ_o) has

been improved greatly. This could be due to the fact that the degree of cure is quite sensitive to the temperature non-uniformity. In this example, the objective function Eq. (4.3) and the constraint Eq. (4.6) are replaced by the following forms, respectively;

$$\psi_o : \text{Maximum } [\int_o^h \alpha^2 dz - (\int_o^h \alpha dz)^2/h], \tag{4.11}$$

$$\psi_3 : [\int_o^h \alpha^2 \, dz - (\int_o^h \alpha dz)^2/h] \leq b, \qquad 0 \leq t \leq \tau. \tag{4.12}$$

The optimal cure cycle of Example 2 is used as the initial trial solution in this case. Fifty five more iterations are required to have the algorithm converged to the optimal solution. The optimal cure cycle shown in Fig. 4.12 has the characteristic of a ramp-hold-ramp feature. Numerical results are listed in Table 4.3. The values of the objective functions of Eq. (4.11) for the starting and the optimal cure cycles are compared in Fig. 4.13. The optimal solution reduces the maximal value of the state of cure deviation as expected. However, the differences are not at all significant. The distribution of the state of cure, shown in Fig. 4.4, corresponding to the optimal cure cycle of Example 3, is similar to that of Example 2. The temperature distribution under the optimal cure cycle in this example is also shown in Fig. 4.15. These results indicate that the change of the objective function from Eq. (4.3) to Eq. (4.11) has only minor effects on the uniformity of the state of cure, even though the profiles of the optimal cure cycle designs are quite different.

Example 4.

This is identical to the problem stated in Example 1, except that the maximum state of cure deviation defined by a new objective function (Eq. 4.13) is minimized; the total processing time is allowed for 150 seconds and the initial cure temperature is regarded as an additional design variable.

In this example, the objective function Eq. (4.3) and the constraint Eq. (4.6) are replaced by the following forms, respectively;

$$\psi_o : \underset{0\leq t\leq \tau}{\text{Maximum}} \ (\alpha_o - \alpha_c), \tag{4.13}$$

$$\psi_3 : (\alpha_o - \alpha_c)^2 \leq b, \qquad 0\leq t\leq \tau. \tag{4.14}$$

In this example, the objective function becomes the difference of the degree of cure between the outer surface, α_o, and the center plane, α_c. The optimal design algorithm does not really achieve convergence. However, after the forty-sixth iteration, the changes of the design variables become small, compared to the magnitudes of the design variables and all the constraints are satisfied. The feasible design of the forty-sixth iteration is then regarded as the final design. Numerical results of this example are listed in Table 4.4. The cure temperature profiles and the values of the objective function of Eq. (4.13) for iterations 1, 46, and that of reference [2] are shown in Figs. 4.16 and 4.17, respectively. Note that the cure cycle given in reference [2] is a constant temperature profile with T_c = 423°K. The cure temperature profile of the forty-sixth iteration has the characteristic of a ramp-hold-ramp feature similar to that of Example 3. It is recognized that the high onset cure temperature of the optimal

cure cycle benefits the cure cycle design by initiating the chemical reaction as quick as possible so as to achieve a better state of cure distribution. Similar to the previous case, the final solution of this example does improve the uniformity of the state of cure, though this improvement is insignificant. The final results of the temperature distribution and the degree of cure distribution at the selected instants are shown in Figs. 4.18 and 4.19, respectively.

CHAPTER V

CONCLUDING REMARKS

At the present time, the cure cycle is generally selected by the method of parametric study conducted by either physical experiments or numerical simulation. This type of approach may be costly and inefficient. Therefore, the development of a unified and systematical approach to design the best cure cycle for a given composite material is needed. A unified Computer-Aided Design method is introduced in this thesis to design the best cure cycle for a resin-fiber composite laminate. The characteristics of curing the resin-fiber composite laminate can be simplified as a diffusion-reaction system and a kinetic model of the cure rate of the resin. The proposed CAD method consists of three uncoupled modules: namely, optimization, analysis, and sensitivity calculation. Once the analysis capability of any cure process analysis is established, the optimization and sensitivity calculation modules can be added onto it to constitute a unified CAD method and to generate the optimal cure cycle systematically.

The optimal cure temperature is required to achieve the following:

1. The maximum temperature during cure should be less than 500°K.
2. At the end of the cure process, the cure of the resin should be completed.

3. The state of cure should be uniform during the cure process.

It is shown by numerical examples that this method performs satisfactorily by carefully selecting the optimization formulation.

The finite element discretization is employed to convert the initial-boundary value problem of interest into a set of first order differential equations. These equations are then solved simultaneously by a numerical code called DE. The finite element method provides a systematical method to analyze the temperature and the degree of cure distribution. Note that very good agreements exist between the finite element solutions and the existing solutions.

Two methods, the adjoint variable technique and the direct differentiation method, are studied for the thermal design sensitivity analysis. In general, the adjoint equations can not be solved simultaneously with the original system equations. Therefore, it is difficult for the adjoint variable technique to have the numerical accuracy of the design derivatives equal to that of the state variables. Numerical examples indicate that the direct differentiation method is superior to the adjoint variable technique in terms of accuracy and physical interpretation. In this thesis, the direct differentiation method is used for the optimization algorithm.

The optimization algorithm used in this thesis is a recursive quadratic programming algorithm with an active set strategy, called a linearization method. The main reason to use this linearization method is that it has been proved to be globally convergent. The optimal design of the cure cycles studied in this thesis is to find the optimal cure temperature during the cure process to have the thermosetting resin

cured as uniformly as possible and to secure the cure completeness of the resin at the end of the cure process.

Four optimal design formulations for the optimal cure cycle design of chopped-fiber SMC are studied. The first example deals with the minimum temperature deviation across the thickness during the cure process, and the total process time is 100 seconds. The optimal cure cycle of this example reduces the value of the objective function from the initial design 2,700 to the optimal one 378 units. The second example deals with the same conditions as Example 1 except that the total processing time is extended to 150 seconds. Using the optimal solution of Example 1 as the initial design, the maximum temperature deviation drops from 250 to 110 units. The third example is identical to Example 1, except that the objective function is changed to minimize the degree of cure deviation across the thickness along the cure process and that the total processing time is 150 seconds. The optimal solution reduces the value of the objective function from the initial design 0.04691 to the optimal one 0.03385. The last example deals with the minimization of the difference between the degree of cure of the outer surface and the center plane. The total processing time is 150 seconds and the initial cure temperature is regarded as an additional design variable. This example is different from the previous examples in which the initial temperatures are set to be the room temperature. The optimal cure cycle reduces the degree of cure deviation between the outer surface and the center plane from the initial design 0.8032 to a feasible design 0.6992, and increases the initial cure temperature to 395° K. Comparing the optimal cure cycle with that of reference [2],

the optimal cure cycle does make the state of cure distributed more uniformly during the cure process.

The numerical examples show that the proposed CAD approach is valid. It does improve the degree of cure uniformity. This study also indicates that the total processing time, the initial heating rate and the initial cure temperature have significant effects on the cure uniformity. Enlarging the design space by increasing the total processing time and adding more design variables can further improve the cure cycle design. The long CPU time is a concern in the optimization process. To shorten the CPU time one may use other numerical algorithms, such as an unconditional stable algorithm, which can increase the time step, or the other kind of optimization algorithms, such as the I-DESIGN [17], which does not need line search to accelerate the optimization process.

The proposed CAD scheme can be extended to design an optimal cure cycle for the autoclave processing. Note that, to design a realistic cure process of resin-fiber composite optimally, some modification over the presented simplified SMC model are required. For example, the flow model, the chemo-viscosity and the heat convection should be considered in the analytical model. The total processing time should be regarded as a design variable to enlarge the design space. Moreover, some experiments are necessary to verify the results of the cure cycle designs.

In summary, it is clear and convincing that the optimization is a very promising technique to enhance the capability of designing the optimal cure cycle for the cure process of resin-fiber composite laminate.

REFERENCES

1. Loos, A. C., and Springer, G. S., "Curing of Graphite/Epoxy Composites," AFWAL-TR-83-4040, March, 1983.

2. Barone, M. E., and Caulk, D. A., "The Effect of Deformation and Thermoset Cure on Heat Conduction in a Chopped-Fiber Reinforced Polyester during Compression Molding," International Journal Heat Mass Transfer, Vol. 22, pp. 1021-1032.

3. Haug, E. J., Mani, N. K., and Krishnaswami, P., "Design Sensitivity Analysis and Optimization of Dynamically Driven System," Computer-Aided Analysis and Optimization of Mechanical System Dynamics, (Ed. E. J. Haug) Springer-Verlag, Berlin, Germany, pp. 555-632, 1984.

4. Hsieh, C. C., and Arora, J. S., "Design Sensitivity Analysis and Optimization of Dynamics Response," Computer Methods in Applied Mechanics and Engineering, No. 2, Vol. 43, pp. 195-219, 1984.

5. Biegler, L. T., "Solution of Dynamics Optimization Problems by Successive Quadratic Programming and Orthogonal Allocation," Report No. DRC-06-45-83, Design Research Center, Carnegie-Mellon University, Pittsburgh, PA, 1983.

6. Bryson, A. E., and Ho, Y. C., Applied Optimal Control, Ginn and Co., Massachusetts, 1969.

7. Shampine, L. F. and Gordon, M. K., Computer Solution of Ordinary Differential Equations: The Initial Value Problem, W. H. Freeman and Co., San Francisco, 1975.

8. Loos, A. C., and Dara, P. H., "Modeling the Curing Process of Thick-Section Autoclave Cured Composites," Department of Engineering Science and Mechanics, Virginia Polytechnic Institute and State University, VA, December 1984.

9. Tao, David Da-Juih, "Finite Element Analysis of Thermoelasticity Problem," Ph. D. Dissertation, Department of Civil Engineering, Princeton University, Princeton, N. J., June 1984.

10. Hou, J. W., "Optimal Cure Cycle Design for Autoclave Processing of Thick Composites Laminates: A Feasibility Study," Progress Report, ODU Research Foundation, November 1985.

11. Adelman, H. M., Haftka, R. T., Camarda, C. J., and Walsh, J. L., "Structural Sensitivity Analysis: Methods, Applications and Needs," NASA TM-85827, June 1984.

12. Hsieh, C. C., and Arora, J. S., "Design Sensitivity Analysis and Optimization of Dynamic Response," Technical Report, No. CAD-SS-83.6, Division of Material Engineering, The University of Iowa, Iowa City, 1983.

13. Choi, K. K., Haug, E. J., Hou, J. W., and Sohoni, V. N., "Pshenichny's Linearization Method For Mechanical System Optimization," ASME Journal of Mechanisms, Transmissions, and Automation in Design, No. 1, Vol. 105, pp. 97-103, 1983.

14. Belegundu, A. D., and Arora, J. S., "A Recursive Quadratic Programming Method with Active Set Strategy for Optimal Design," International Journal for Numerical Method in Engineering, Vol. 20, No. 5, pp. 803-816, May 1984.

15. Pshenichny, B. N. and Danilin Y. M., Numerical Methods in External Problems, MIR Publishers, Moscos, 1978.

16. Taylor, J. E., and Bendose, M. P., "A Interpolation for Min-Max Structural Design Problems Including A Method for Relaxing Constraints," International Journal of Solids Structures, No. 4, Vol. 20, pp. 301-314, 1984.

17. Arora, J. S., Thanedar, P. B., and Tseng, C. H., "User's Manual for Program IDESIGN," Technical Report No. 85-10, Optimal Design Laboratory, College of Engineering, The University of Iowa, Iowa City, Iowa 52242, 1985.

APPENDICES

APPENDIX A

FINITE ELEMENT MATRIX EQUATIONS FOR A DIFFUSION-REACTION SYSTEM

The equations (2.12) - (2.13) can be rewritten here:

$$0 = \sum_{1}^{NE} \int_{z_i}^{z_{i+1}} (\rho c \dot{T} u + k T' u' + \rho c \dot{T}_c u - \rho H r f u)\, dz, \qquad (A.1)$$

and

$$0 = \sum_{1}^{NE} \int_{z_i}^{z_{i+1}} (\dot{\alpha} - f)\, v\, dz \qquad (A.2)$$

where NE denotes the number of elements and u(z) and v(z) are the testing functions.

According to the Galerkin method, the arbitrary interpolation functions N_j and L_j defined in Eqs. (2.8) and (2.10) can be considered as u(z) and v(z), respectively. Furthermore, the temperature and the degree of cure can be expressed as linear combinations of interpolation functions and the nodal values as shown in Eqs. (2.9) and (2.11). One may then write a matrix equation for the first integral of Eq. (A.1) defined as

$$\int_{z_i}^{z_{i+1}} \rho c \dot{T} u \, dz$$

$$= \int_{0}^{\ell_i} \rho c \, N_j \, \underline{N}^T \, d\bar{z} \, \dot{\underline{T}}, \qquad j=1,2,3,4. \tag{A.3}$$

where z denotes the global coordinate system, $\bar{z}$ denotes the local coordinate system, $\bar{z} = z - z_i$, and $\ell_i = z_{i+1} - z_i$. Let a vector $\underline{C}$ be defined as

$$\underline{C}_j^T = \int_{0}^{\ell_i} N_j \, \underline{N}^T \, d\bar{z}, \qquad j = 1,2,3,4.$$

Consequently, one has

$$\int_{z_i}^{z_{i+1}} \rho c \dot{T} u \, dz$$

$$= \rho \, c \, \underline{C}_j^T \dot{\underline{T}} \tag{A.4}$$

for $j = 1$ to 4. At this moment, one may introduce an element matrix $[C]^i$ in the following way:

$$[C]^i = \int_{0}^{\ell_i} \underline{N} \, \underline{N}^T \, d\bar{z}$$

$$= [\underline{C}_1, \underline{C}_2, \underline{C}_3, \underline{C}_4]^T$$

where the vector $\underline{C}_j$ is defined in Eq. (A.4). It is understood that $[C]^i$ is symmetric. Thus, for $u = N_j$ with $j = 1$ to 4, one has

$$\int_{z_i}^{z_{i+1}} \rho c \dot{T} u \, dz$$

$$= \rho c \, [C]^i \, \dot{\underline{T}} \qquad (A.5)$$

Similarly, using the following definitions for an element matrix $[K]^i$ and a vector $\underline{P}^i$:

$$[K]^i = \int_0^{\ell_i} \underline{N}' \, \underline{N}'^T \, d\bar{z}, \qquad (A.6)$$

and

$$\underline{P}^i = \int_0^{\ell_i} \underline{N} \, d\bar{z} \qquad (A.7)$$

one obtains matrix equations for the second and third integrals of Eq. (A.1) as

$$\int_{z_i}^{z_{i+1}} kT' u' \, dz$$

$$= k \, [K]^i \, \underline{T} \qquad (A.8)$$

and

$$\int_{z_i}^{z_{i+1}} \rho c \, \dot{T}_c \, u \, dz$$

$$= \rho c \, \underline{P}^i \, \dot{T}_c . \qquad (A.9)$$

The element matrices $[K]^i$, $[C]^i$ and $\underline{P}^i$ can be expressed explicitly in terms of the length of element i, ℓ_i, as follows:

$$[K]^i = \begin{bmatrix} \frac{6}{5\ell_i} & \frac{1}{10} & -\frac{6}{5\ell_i} & \frac{-1}{10} \\ & \frac{2\ell_i}{15} & \frac{1}{10} & \frac{\ell_i}{30} \\ \text{Sym.} & & \frac{6}{5\ell_i} & -\frac{1}{10} \\ & & & \frac{2\ell_i}{15} \end{bmatrix} \tag{A.10}$$

$$[C]^i = \frac{\ell_i}{420} \begin{bmatrix} 156 & 22\ell_i & 54 & 13\ell_i \\ & 4\ell_i^2 & 13\ell_i & -3\ell_i^2 \\ \text{Sym.} & & 156 & -22\ell_i^2 \\ & & & 4\ell_i^2 \end{bmatrix} \tag{A.11}$$

and

$$\underline{P}^i = \{\ell_i/2,\ \ell_i^2/12,\ \ell_i/2,\ -\ell_i^2/12\}^T \tag{A.12}$$

Following the previous derivation, for $v = L_j$ with $j = 1, 2$, one may write a matrix equation for the first integral of Eq. (A.2) as

$$\int_{z_i}^{z_{i+1}} \dot{\alpha} v \, dz$$

$$= \int_0^{\ell_i} L_j \, \underline{L}^T \, d\bar{z} \, \dot{\underline{\alpha}} \tag{A.13}$$

where L_j is a shape function for the degree of cure. Let an element matrix $[M]^i$ be defined as

$$[M]^i = \int_0^{\ell_i} \underline{L}\,\underline{L}^T \, d\bar{z}. \tag{A.14}$$

Thus, for $v = L_j$ with j=1, 2, one has the following identity:

$$\int_{z_i}^{z_{i+1}} \dot{\alpha}\, v \, dz$$

$$= [M]^i \, \underline{\dot{\alpha}}. \tag{A.15}$$

The matrix [M] for the ith element can be derived explicitly in terms of ℓ_i as

$$[M]^i = \begin{bmatrix} \ell_i/3 & \ell_i/6 \\ \ell_i/6 & \ell_i/3 \end{bmatrix}. \tag{A.16}$$

After substituting an interpolation function for the trial function u(z), the last term in Eq. (A.1) yields a scalar Q_{ip} for ith element as

$$Q_{ip} = \int_0^{\ell_i} \rho H r f(\alpha,T,T_c)\, N_p(z)\, d\bar{z}, \qquad p = 1,2,3,4. \tag{A.17}$$

In a similar fashion, the discretized form of the last term in Eq. (A.2) can be expressed as

$$R_{iq} = \int_0^{\ell_i} f(\alpha,T,T_c)\, L_q(z)\, d\bar{z}, \qquad q = 1,2. \tag{A.18}$$

The cure rate $\dot{\alpha} = f(\alpha,T,Tc)$ in Q_{ip} and R_{iq} is a function of the temperature and the degree of cure defined in Eq. (2.5). Note that the temperature distribution has been replaced by $T+T_c$. Thus, Eq. (2.5) becomes

$$\dot{\alpha} = f(\alpha,T,T_c)$$

$$= (a_1 e^{-d_{1/R(T+T_c)}} + a_2 e^{-d_{2/R(T+T_c)}} \alpha^m)(1-\alpha)^n. \qquad (A.19)$$

Within the ith element, i.e., $z_i \leq z \leq z_{i+1}$, the distributions of temperature is interpolated by shape functions and nodal variables as defined in Eq. (2.9). To abbreviate the notations, the following Γ is introduced:

$$\Gamma = T(z,t) + T_c(t)$$

$$= \underline{N}^T \underline{T} + T_c(t) \qquad (A.20)$$

It is also understood that

$$\alpha(z,t) = \underline{L}^T \underline{\alpha}. \qquad (A.21)$$

Hence, Q_{ip} and R_{iq} can be expressed as

$$Q_{ip} = \rho Hr \int_o^{\ell_i} (a_1 e^{-d_{1/R\Gamma}} + a_2 e^{-d_{2/R\Gamma}} \alpha^m)(1-\alpha)^n N_p(z)d\bar{z}, \quad p = 1,2,3,4.$$

and

$$R_{iq} = \int_o^{\ell_i} (a_1 e^{-d_{1/R\Gamma}} + a_2 e^{-d_{2/R\Gamma}} \alpha^m)(1-\alpha)^n L_q(z)d\bar{z}, \quad q = 1,2$$

where Q_{ip} and R_{iq} are components of a 4 x 1 load vector $\underline{Q}$ and a 2 x 1 load vector $\underline{R}$, respectively. Note that it is difficult to evaluate the above equations analytically because of the complexity. However, using Eqs. (A.20) - (A.21), the Q_{ip} and R_{iq} can be computed numerically provided that the nodal values of $\underline{T}$ and $\underline{\alpha}$ are known. The numerical examples represented in Section 2.3 are solved by using the Simpson's rule for this numerical integration. The element matrix equations of Eqs. (A.1) and (A.2) for the ith element can then be shown as

$$\rho c[C]^i \dot{\underline{T}} + k[K]^i \underline{T} + \rho c \underline{P}^i \dot{T}_c = \underline{Q}^i, \tag{A.22}$$

$$[M]^i \dot{\underline{\alpha}} = \underline{R}^i, \tag{A.23}$$

Finally, these element matrix equations can be assembled into a set of global system equations in a matrix form as

$$\rho c[C] \dot{\underline{T}} + k[K] \underline{T} + \rho c \underline{P} \dot{T}_c = \underline{Q} \tag{A.24}$$

$$[M]\dot{\underline{\alpha}} = \underline{R} \tag{A.25}$$

APPENDIX B

FINITE ELEMENT MATRIX EQUATIONS OF THERMAL DESIGN SENSITIVITY ANALYSIS BY USING THE DIRECT DIFFERENTIATION METHOD

The given equation (A.19) can be rewritten here:

$$\dot{\alpha} = f(\alpha, T, T_c)$$

$$= (a_1 e^{-d_{1/R(T+T_c)}} + a_2 e^{-d_{2/R(T+T_c)}} \alpha^m)(1-\alpha)^n. \qquad (B.1)$$

Following the definition of the direct differentiation method, one takes derivatives of the above differential equation with respect to a single design variable directly to obtain

$$\frac{d\dot{\alpha}}{db} = \frac{df}{db}$$

$$= \frac{\partial f}{\partial \alpha}\frac{d\alpha}{db} + \frac{\partial f}{\partial T}\frac{dT}{db} + \frac{\partial f}{\partial T_c}\frac{dT_c}{db}. \qquad (B.2)$$

Since f is an explicit function of α, T, and T_c, one can find

$$\frac{\partial f}{\partial \alpha} = -n(a_1 e^{-d_{1/R(T+T_c)}} + a_2 e^{-d_{2/R(T+T_c)}} \alpha^m)(1-\alpha)^{n-1}$$

$$+ ma_2 e^{-d_{2/R(T+T_c)}} \alpha^{m-1} (1-\alpha)^n \qquad (B.3)$$

and

$$\frac{\partial f}{\partial T} = \frac{1}{R(T+T_c)^2} (a_1 d_1 e^{-d_{1/R(T+T_c)}} + a_2 d_2 e^{-d_{2/R(T+T_c)}} \alpha^m)(1-\alpha)^n$$

$$= \frac{\partial f}{\partial T_c}$$

the equations (3.22) and 3.23) can be rewritten here as

$$\rho c \dot{T}_b = kT_b'' - \rho c \dot{T}_{cb} + \rho Hr \frac{\partial f}{\partial \alpha} \alpha_b + \rho Hr \frac{\partial f}{\partial T} T_b + \rho Hr \frac{\partial f}{\partial T_c} T_{cb}, \qquad (B.5)$$

and

$$\dot{\alpha}_b = \frac{\partial f}{\partial \alpha} \alpha_b + \frac{\partial f}{\partial T} T_b + \frac{\partial f}{\partial T_c} T_{cb}. \qquad (B.6)$$

It is assumed that $T_b(z,b,t)$ and $\alpha_b(z,b,t)$ have the same regularity as $T(z,b,t)$ and $\alpha(z,b,t)$. Thus, the shape functions of $T(z,b,t)$ and $\alpha(z,b,t)$ can be employed here to interpolate the $T_b(z,b,t)$ and $\alpha(z,b,t)$, i.e.

$$T_b(z,b,t) = \underline{N}^T(z)\, \underline{T}_b, \qquad (B.7)$$

and

$$\alpha_b(z,b,t) = \underline{L}^T(z)\, \underline{\alpha}_b. \qquad (B.8)$$

where $\underline{N}(z)$ and $\underline{L}(z)$ are defined in Eqs. (2.8) and (2.10), and $\underline{T}_b$ and $\underline{\alpha}_b$ are the vectors of nodal values of $T_b(z,b,t)$ and $\alpha_b(z,b,t)$.

Based on the same derivation discussed in Appendix A, the global matrix equations for Eqs. (B.5) and (B.6) can be shown as

$$\rho c\,[C]\,\dot{\underline{T}}_b + k[K]\,\underline{T}_b + \rho c\,\underline{P}\,\dot{T}_{cb} = \bar{\underline{Q}}, \tag{B.9}$$

and

$$M]\,\dot{\underline{\alpha}}_b = \bar{\underline{R}} \tag{B.10}$$

where matrices [C], [K], [M], and $\underline{P}$ are the same as those given in Eqs. (A.10)-(A.13) and (A.16), and the components of $\bar{\underline{Q}}$ and $\bar{\underline{R}}$ for the ith element are evaluated as

$$\bar{Q}_{ip} = \rho Hr \int_0^{\ell_i} \left(\frac{\partial f}{\partial \alpha}\,\alpha_b + \frac{\partial f}{\partial T}\,T_b + \frac{\partial f}{\partial T_c}\,T_{cb}\right) N_p(z)\,d\bar{z}, \qquad p = 1,2,3,4. \tag{B.11}$$

and

$$\bar{R}_{iq} = \int_0^{\ell_i} \left(\frac{\partial f}{\partial \alpha}\,\alpha_b + \frac{\partial f}{\partial T}\,T_b + \frac{\partial f}{\partial T_c}\,T_{cb}\right) L_q(z)\,d\bar{z}, \qquad q = 1,2. \tag{B.12}$$

The N(z) and L(z) in the above equations are the shape functions which interpolate the design derivatives of the temperature and the state of cure, respectively. Note that it is difficult to calculate Eqs. (B.11)-(B.12) analytically because of complexity. However, the $\bar{Q}_{ip}$ and $\bar{R}_{iq}$ can be computed numerically provided that the nodal values of $\underline{T}$, $\underline{\alpha}$, $\underline{T}_b$, and $\underline{\alpha}_b$ are known.

TABLES

Table 2.1 Material Properties

ρ	$= 1900$ kg m^{-3}
c	$= 1.0$ J g^{-1} k^{-1}
k	$= 0.53$ W m^{-1} k^{-1}
a_1	$= 4.9 \times 10^{14}$ sec^{-1}
a_2	$= 6.2 \times 10^{5}$ sec^{-1}
d_1	$= 140$ kJ $mole^{-1}$
d_2	$= 51$ kJ $mole^{-1}$
m	$= 1.3$
n	$= 2.7$
R	$= 8.83138$ J $mole^{-1}$ K^{-1}
Hr	$= 84$ J g^{-1}

Table 4.1 Convergence History of Optimum Design (Example 1)

	Initial Value	Final Value
Design Variables:		
b_1	100.	115.74
b_2	100.	100.52
b_3	100.	-5.16
b_4	100.	6.83
cost function	2,700.	378.33
ℓ^2 norm	33.62	0.0054
Computer Time (on CDC 855)	---	108,140 CPU sec.
No. of Iterations	---	22

Table 4.2 Convergence History of Optimum Design (Example 2)

	Initial Value	Final Value
Design Variables:		
b_1	115.74	162.32
b_2	100.52	30.98
b_3	-5.16	-0.18
b_4	6.83	5.00
cost function	250.00	110.86
ℓ^2 norm	40.88	0.0147
Computer Time (on CDC 855)	---	156,370 CPU sec.
No. of Iterations	---	25

Table 4.3 Convergence History of Optimum Design (Example 3)

	Initial Value	Final Value
Design Variables:		
b_1	162.32	200.42
b_2	30.98	25.04
b_3	-0.18	46.99
b_4	5.00	-5.28
cost function x 10^3	46.91	33.85
ℓ^2 norm	5.29	0.19
Computer Time (on CDC 855)	---	319,000 CPU sec.
No. of Iterations	---	55

Table 4.4 Convergence History of Optimum Design (Example 4)

	Initial Value	Final Value
Design Variables:		
To	300.00	395.85
b_1	168.39	106.59
b_2	47.41	-46.92
b_3	40.67	23.42
b_4	-0.99	-24.29
cost function	0.8032	0.6992
ℓ^2 norm	111.40	4.08788
Computer Time (on IBM 4381)	---	196,800 CPU sec.
No. of Iterations	---	46

FIGURES

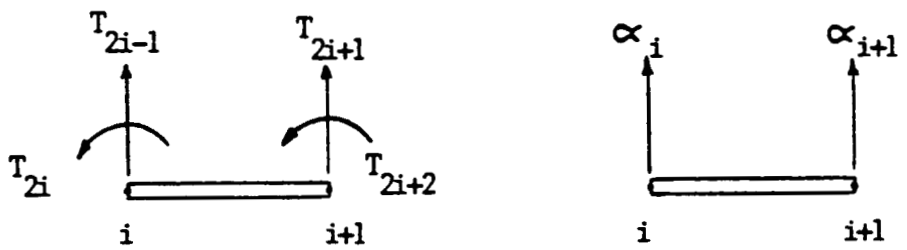

Figure 2.1 Finite Element Discretization.

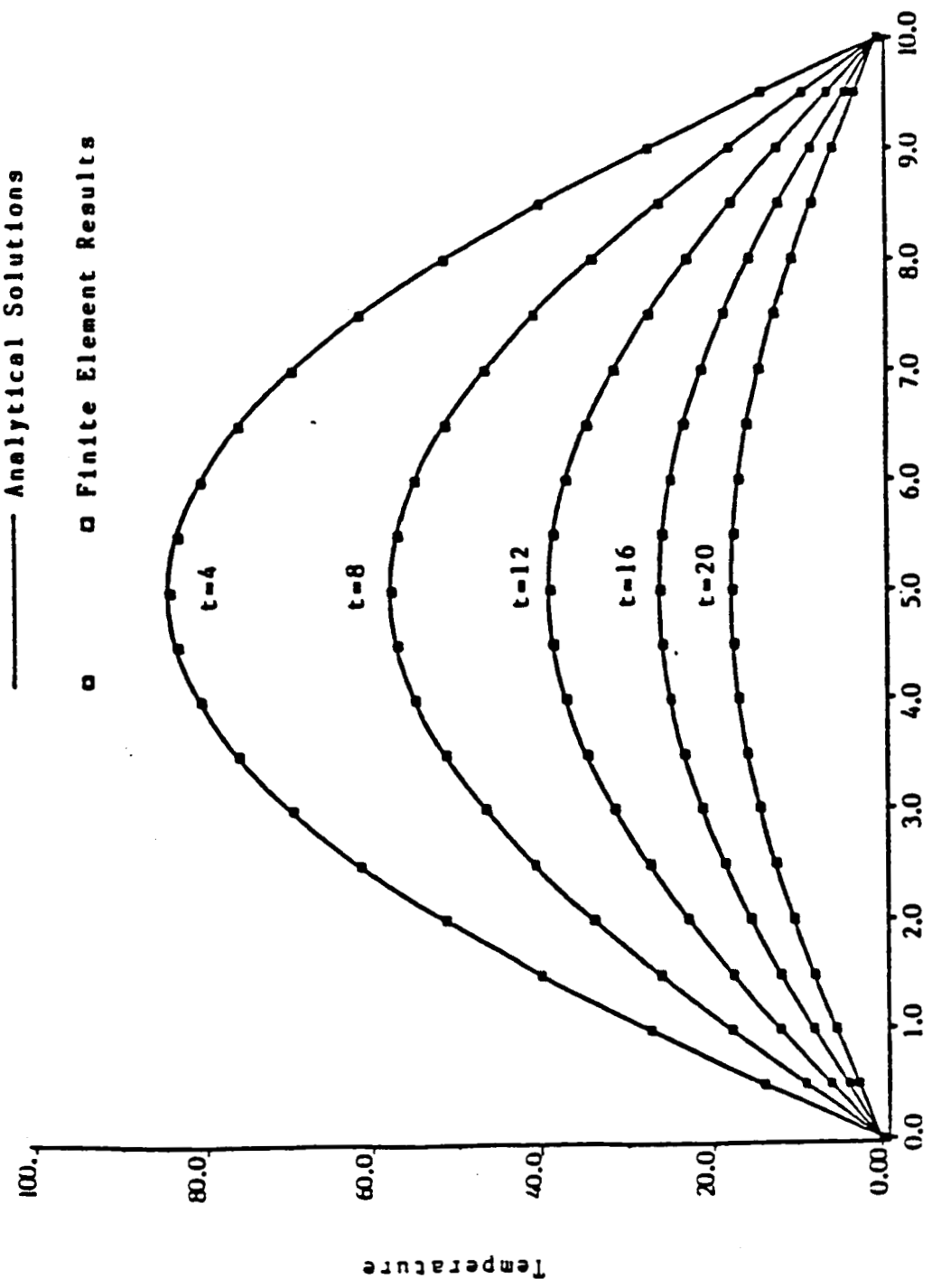

Figure 2.2 One Dimensional Heat Conduction with Prescribed End Temperature: Spatial Temperature Distribution.

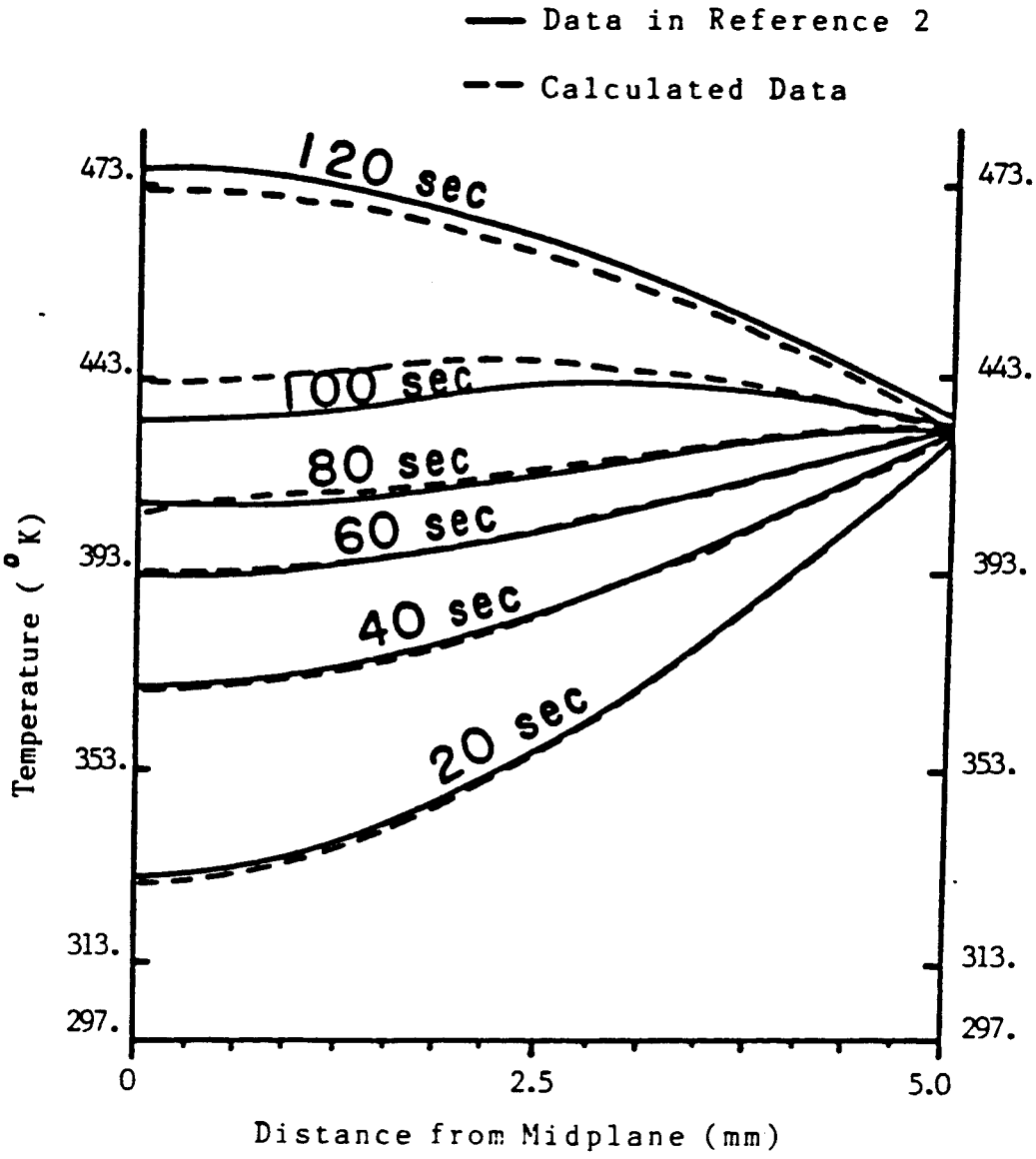

Figure 2.3 Temperature Profiles for 10-mm Thick Sheet.

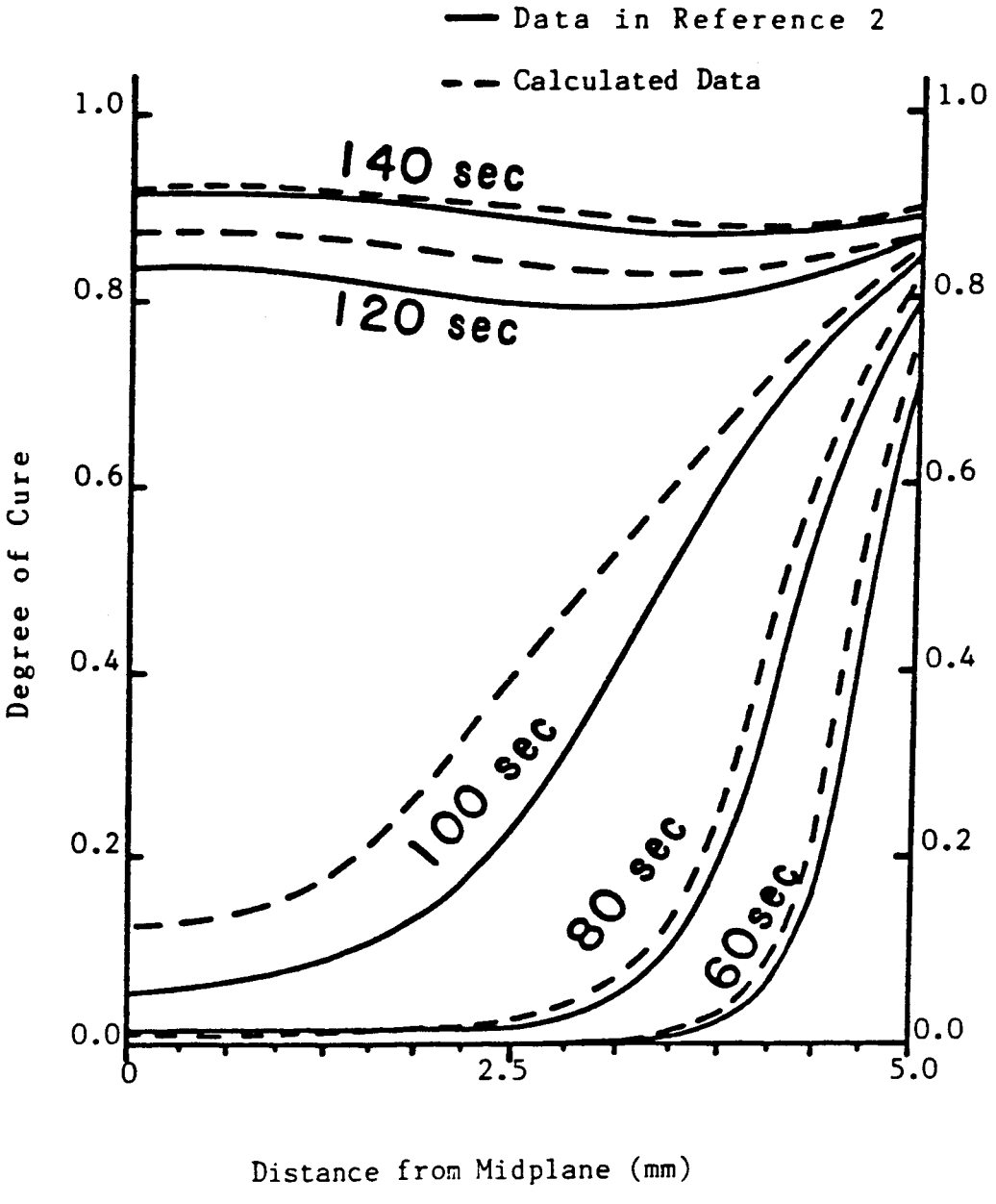

Figure 2.4 Cure Profiles for 10-mm Thick Sheet.

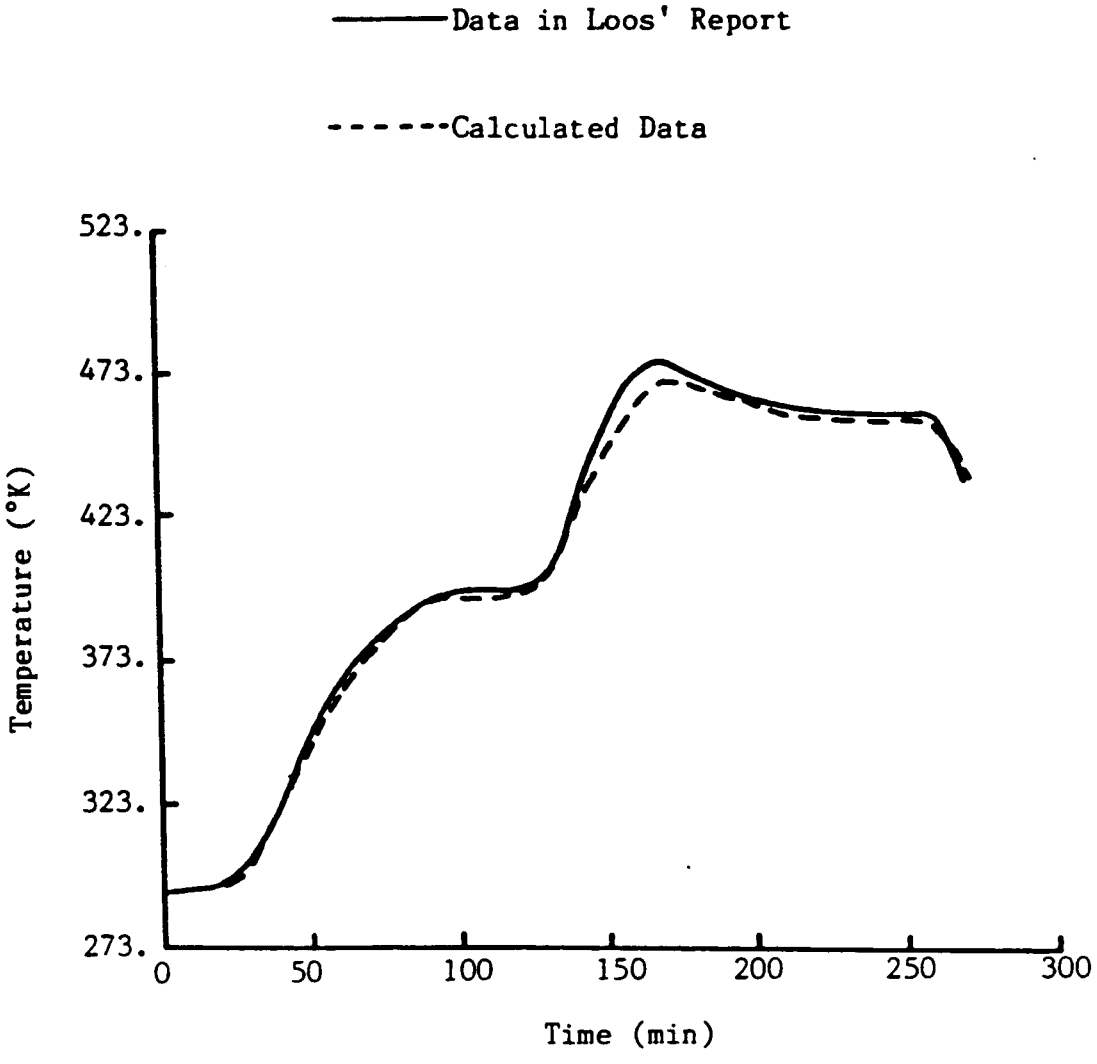

Figure 2.5 Temperature Profile at the Center of Laminate for Thick Section Autoclave Cured Composite.

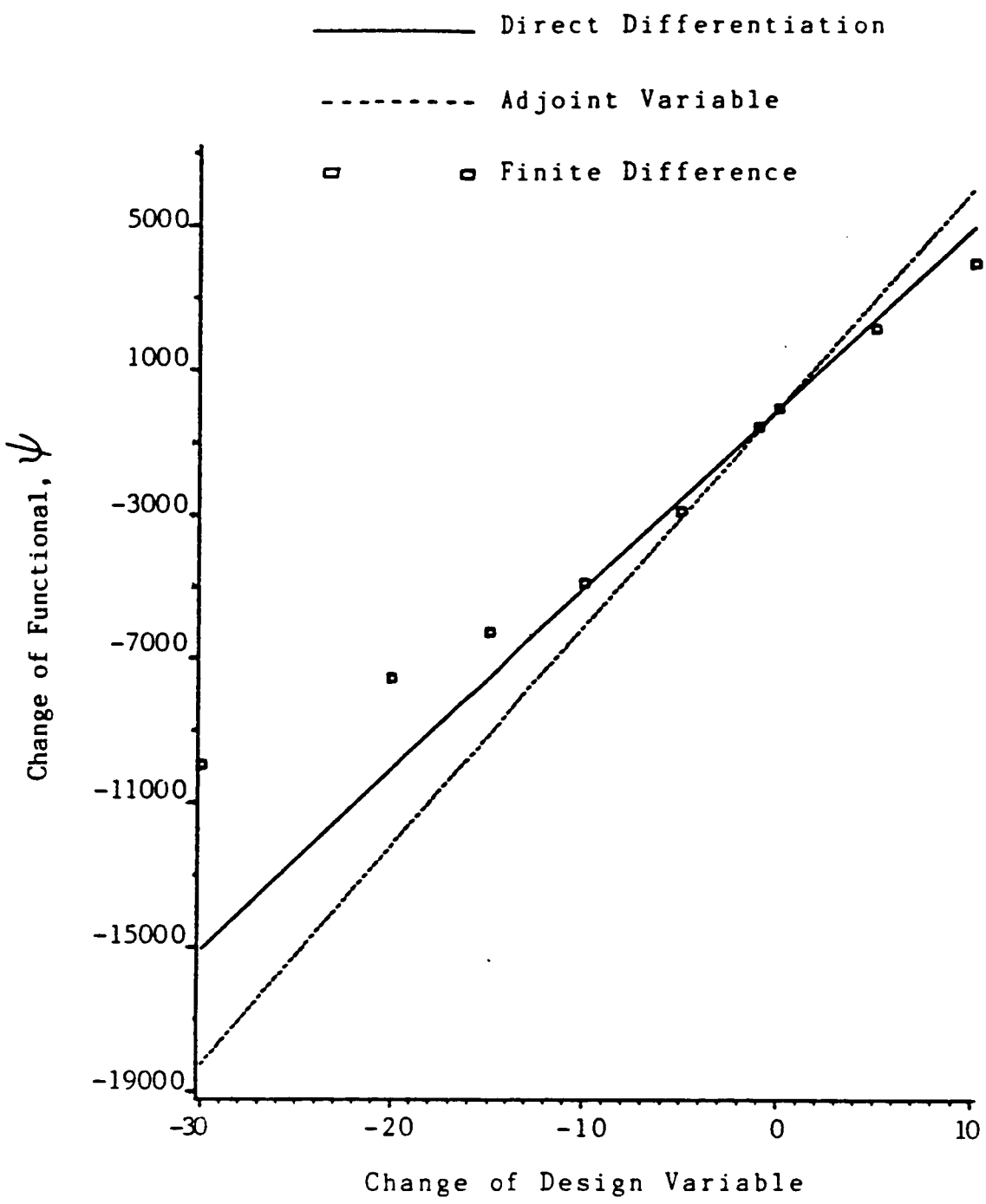

Figure 3.1 Thermal Design Derivatives for Press Molding with Respect to the Mold Temperature.

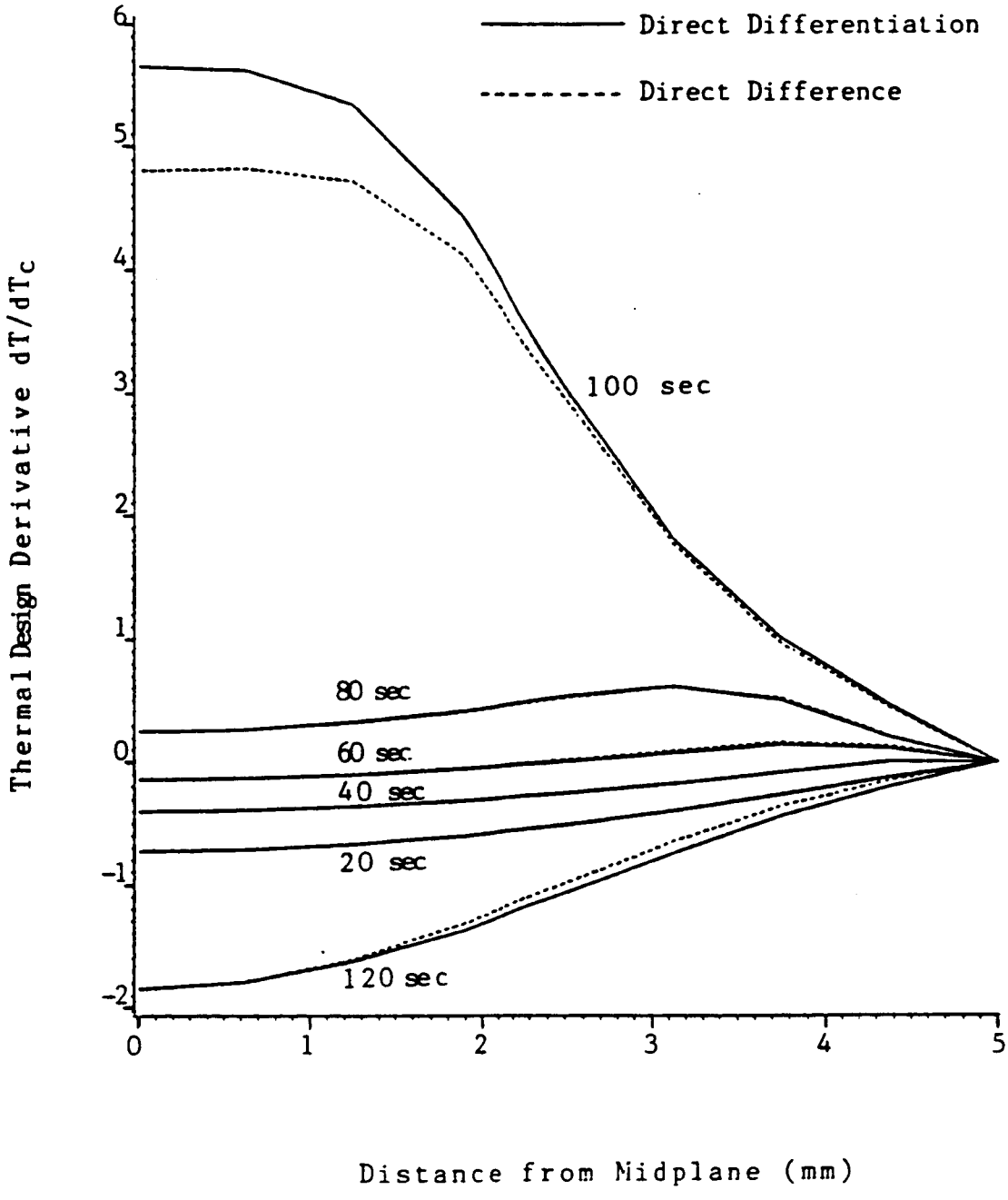

Figure 3.2 Profiles of Thermal Design Derivatives of Temperature with Respect to the Mold Temperature.

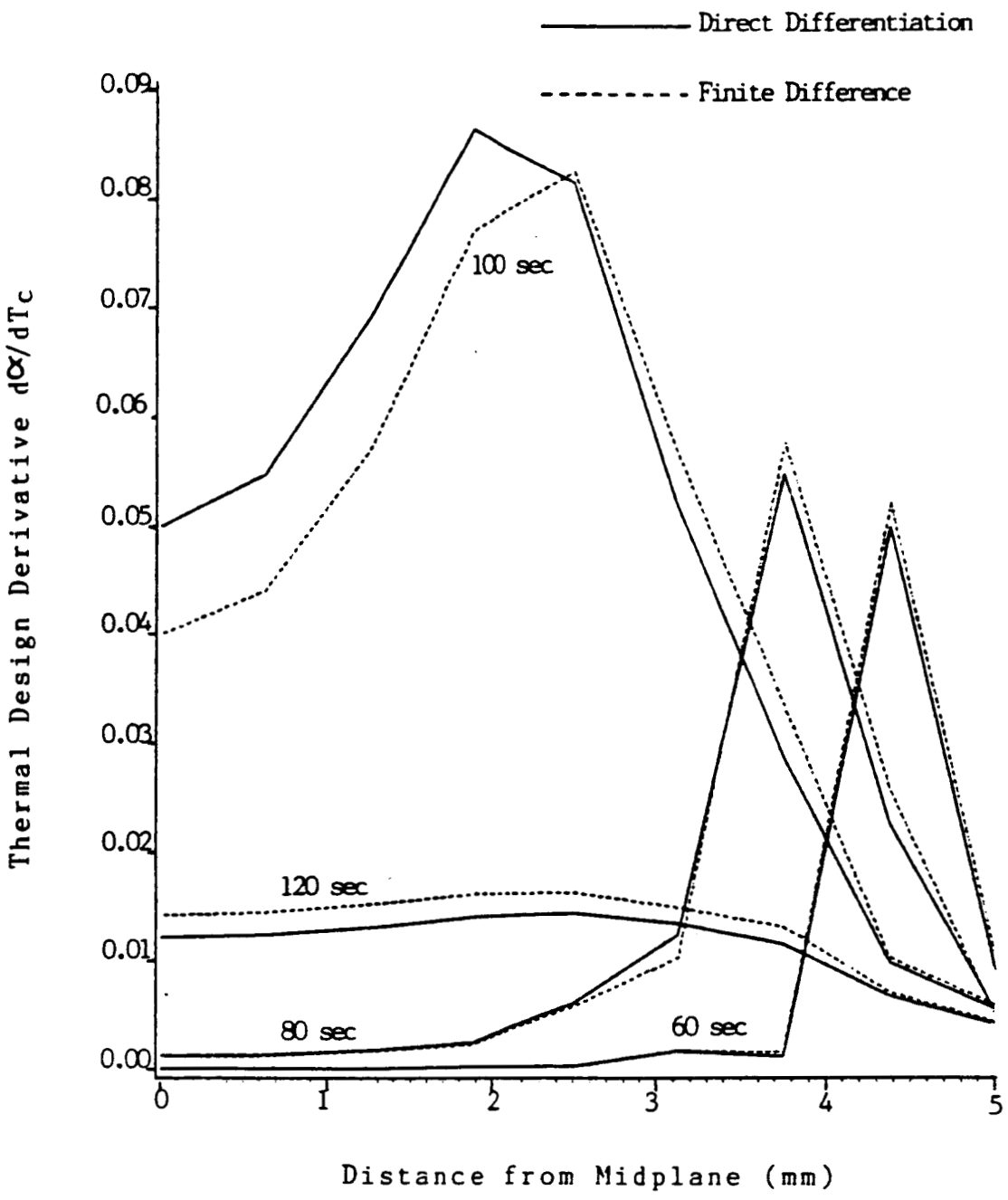

Figure 3.3 Profiles of Thermal Design Derivatives of the State of Cure with Respect to the Mold Temperature.

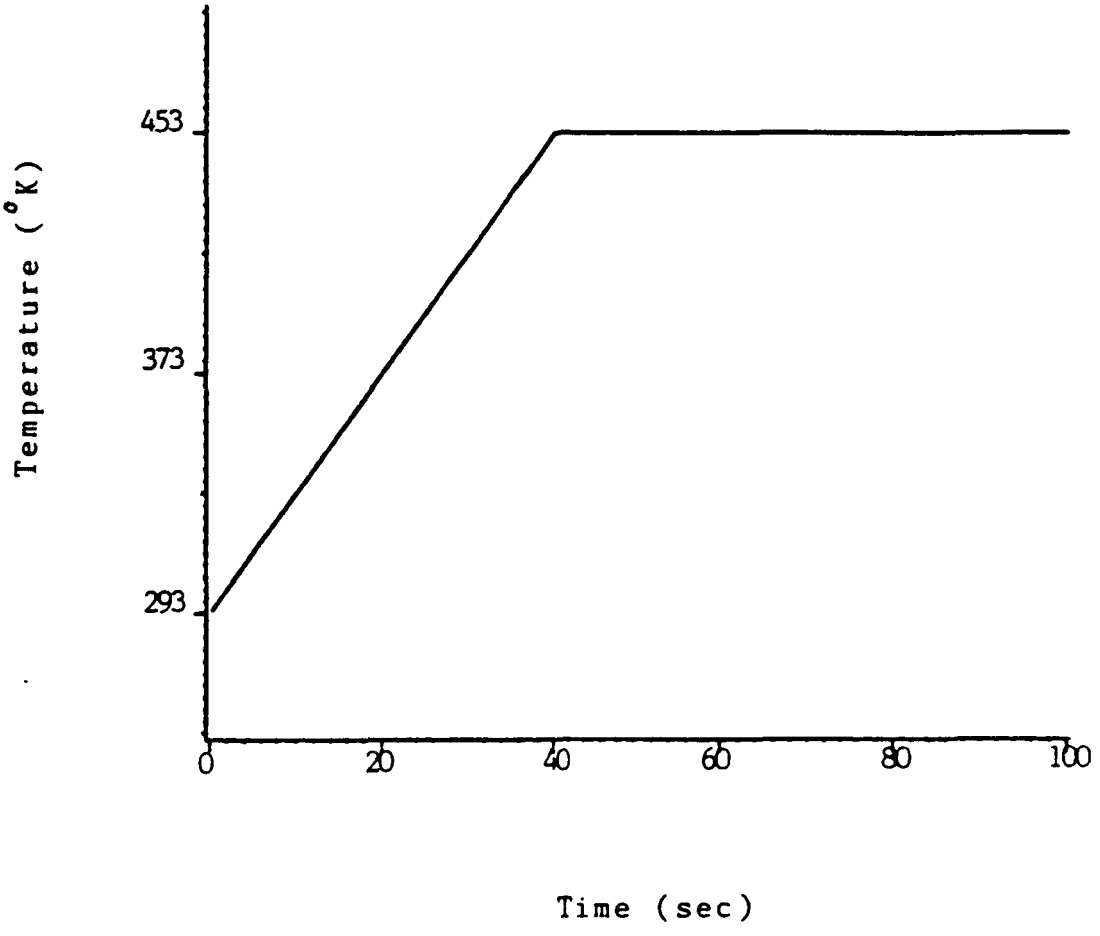

Figure 3.4 The Cure Temperature for Compression Molding.

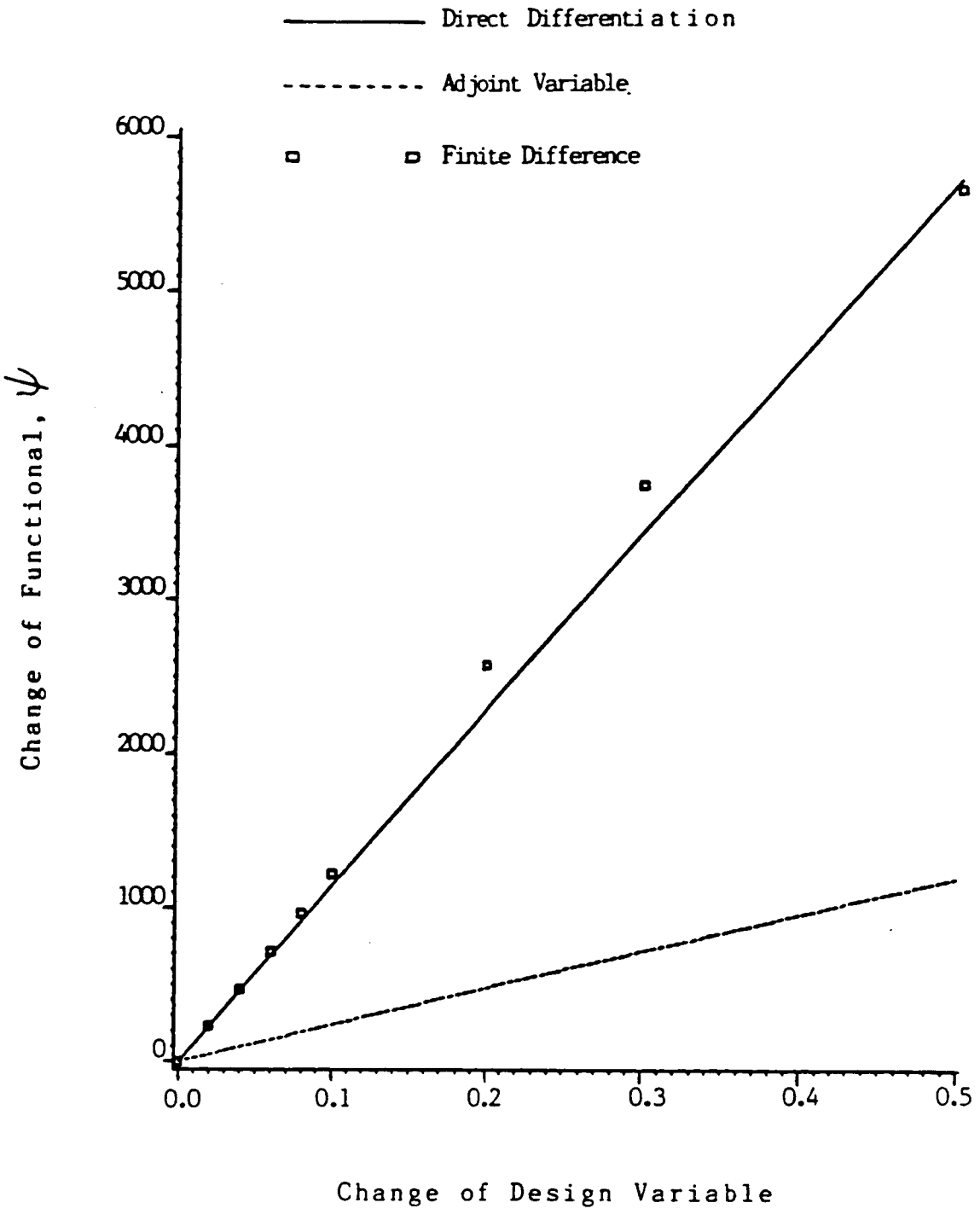

Figure 3.5 Thermal Design Derivatives for Press Molding with Respect to the Heating Rate.

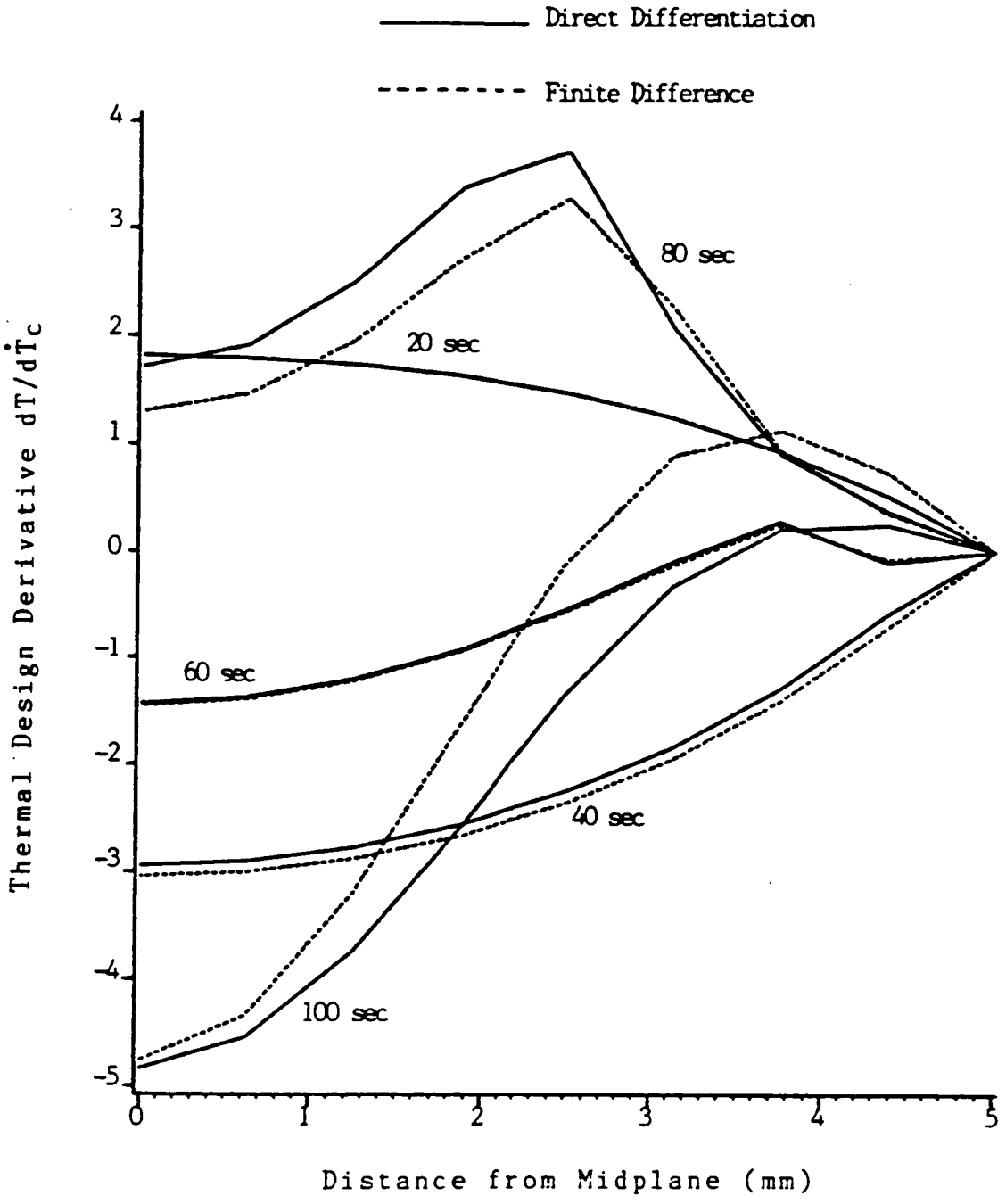

Figure 3.6 Profiles of Thermal Design Derivatives of Temperature with Respect to the Heating Rate.

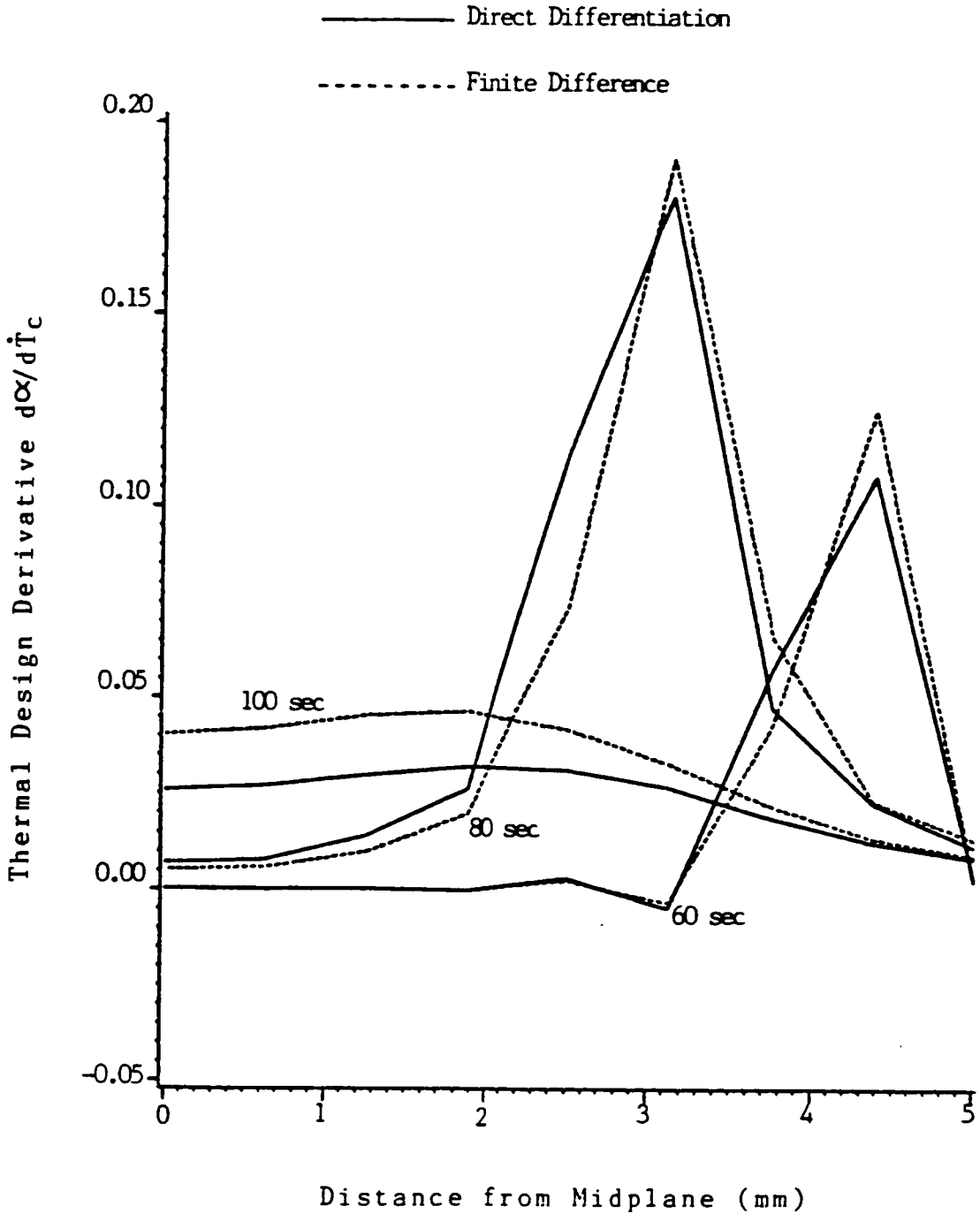

Figure 3.7 Profiles of Thermal Design Derivatives of the State of Cure with Respect to the Heating Rate.

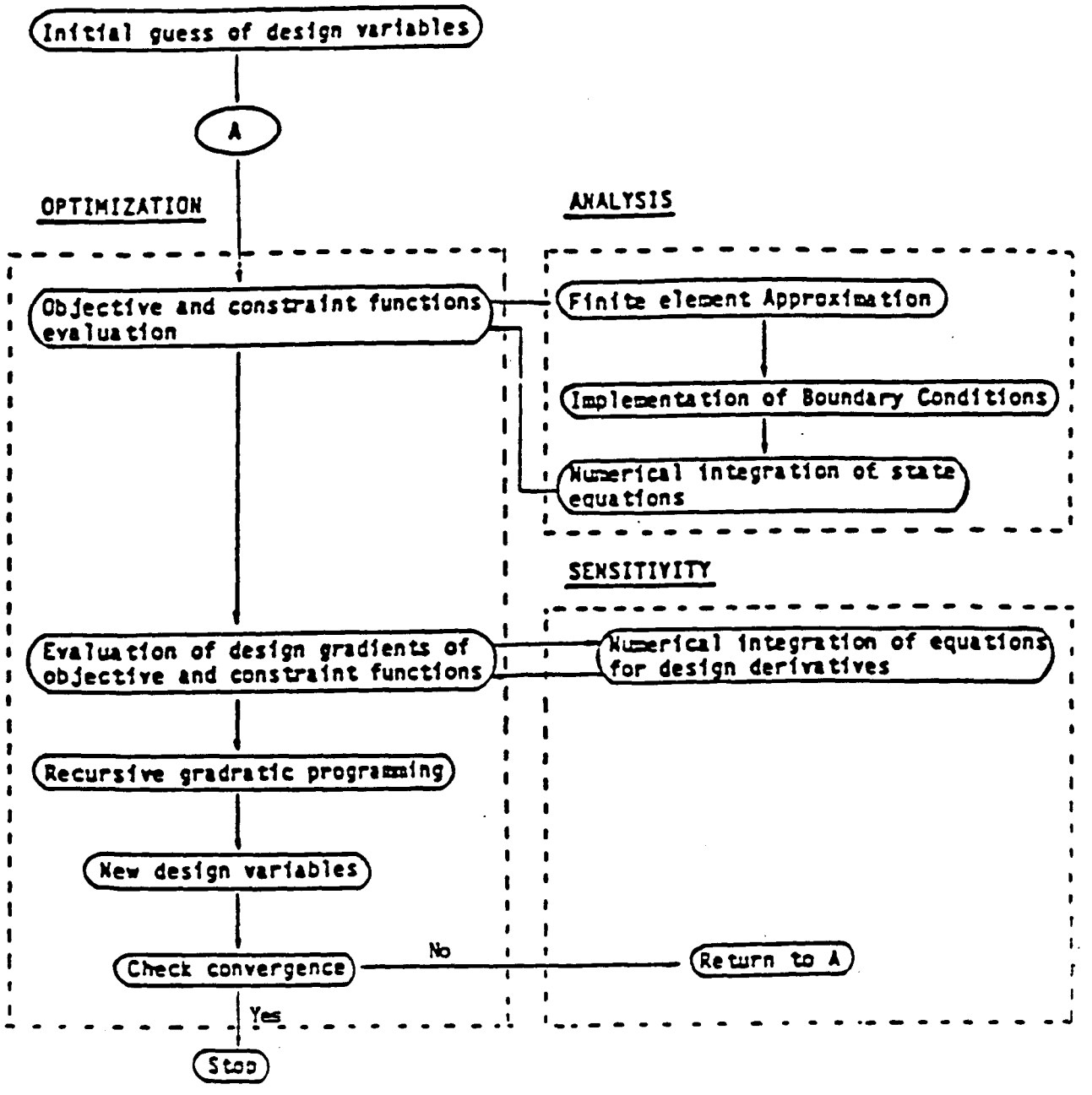

Figure 4.1 Flow Chart of the Proposed CAD Method.

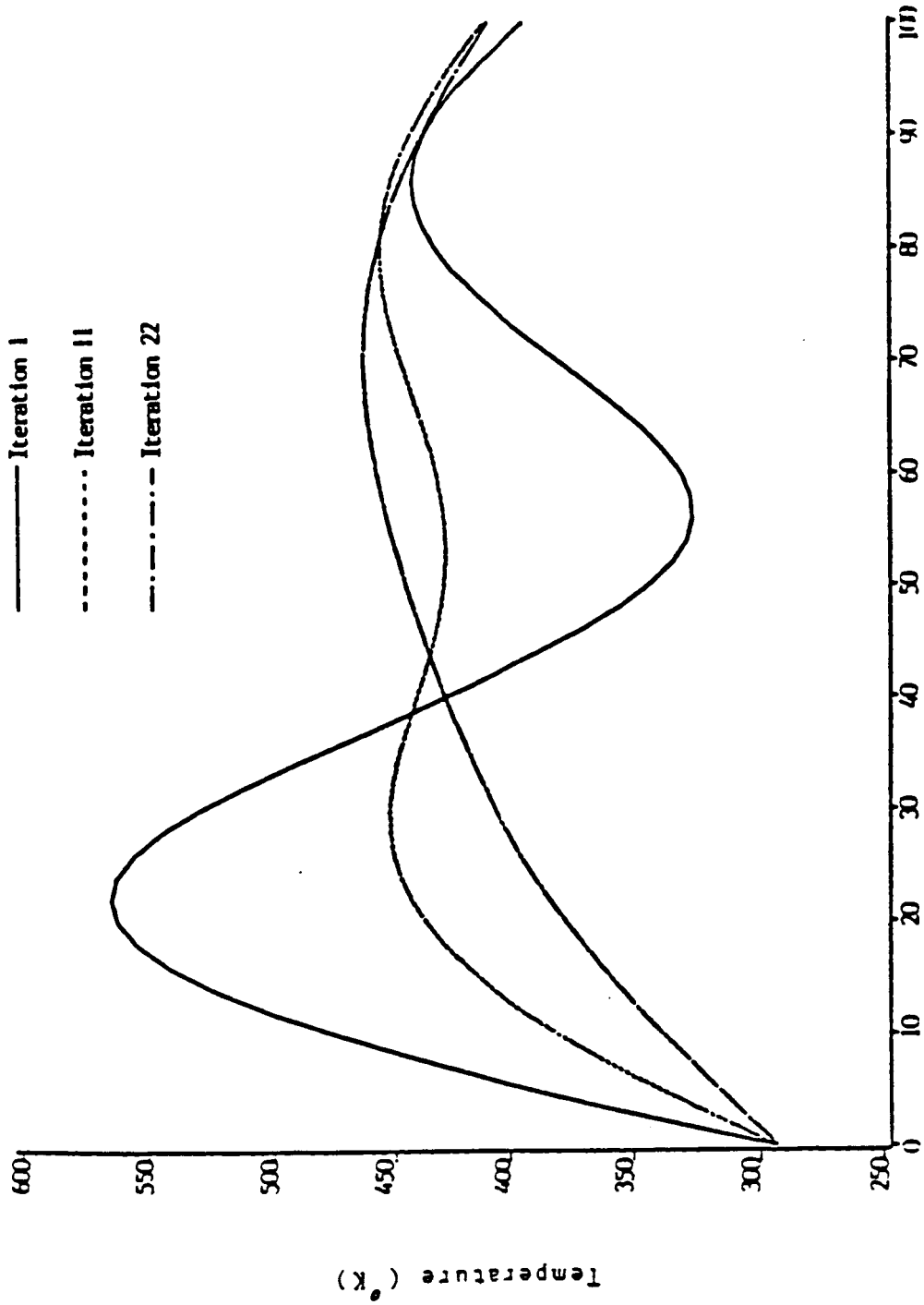

Figure 4.2 Example 1: Profiles of the Cure Temperature.

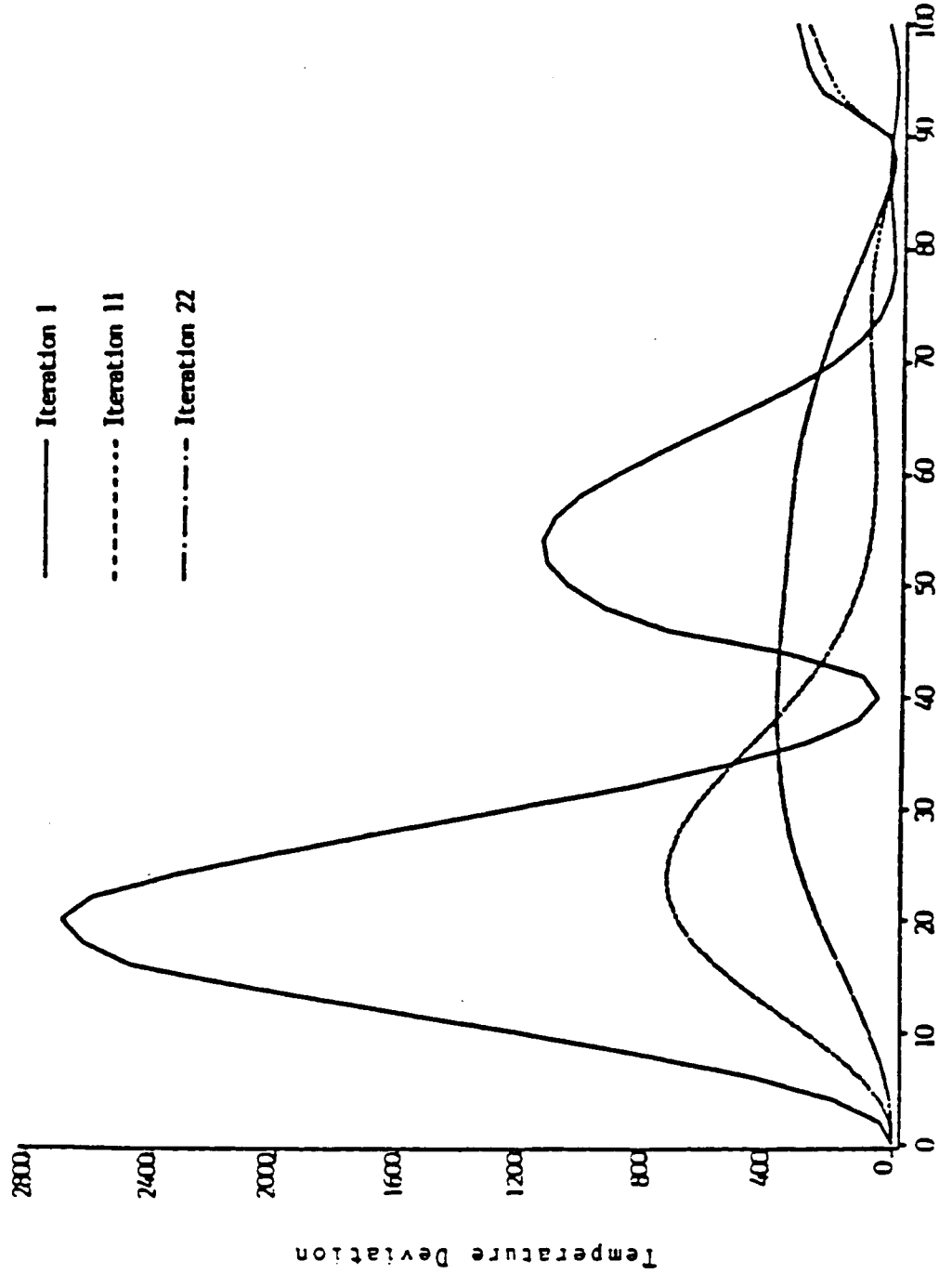

Figure 4.3 Example 1: Profiles of the Least-Squared Temperature Deviation.

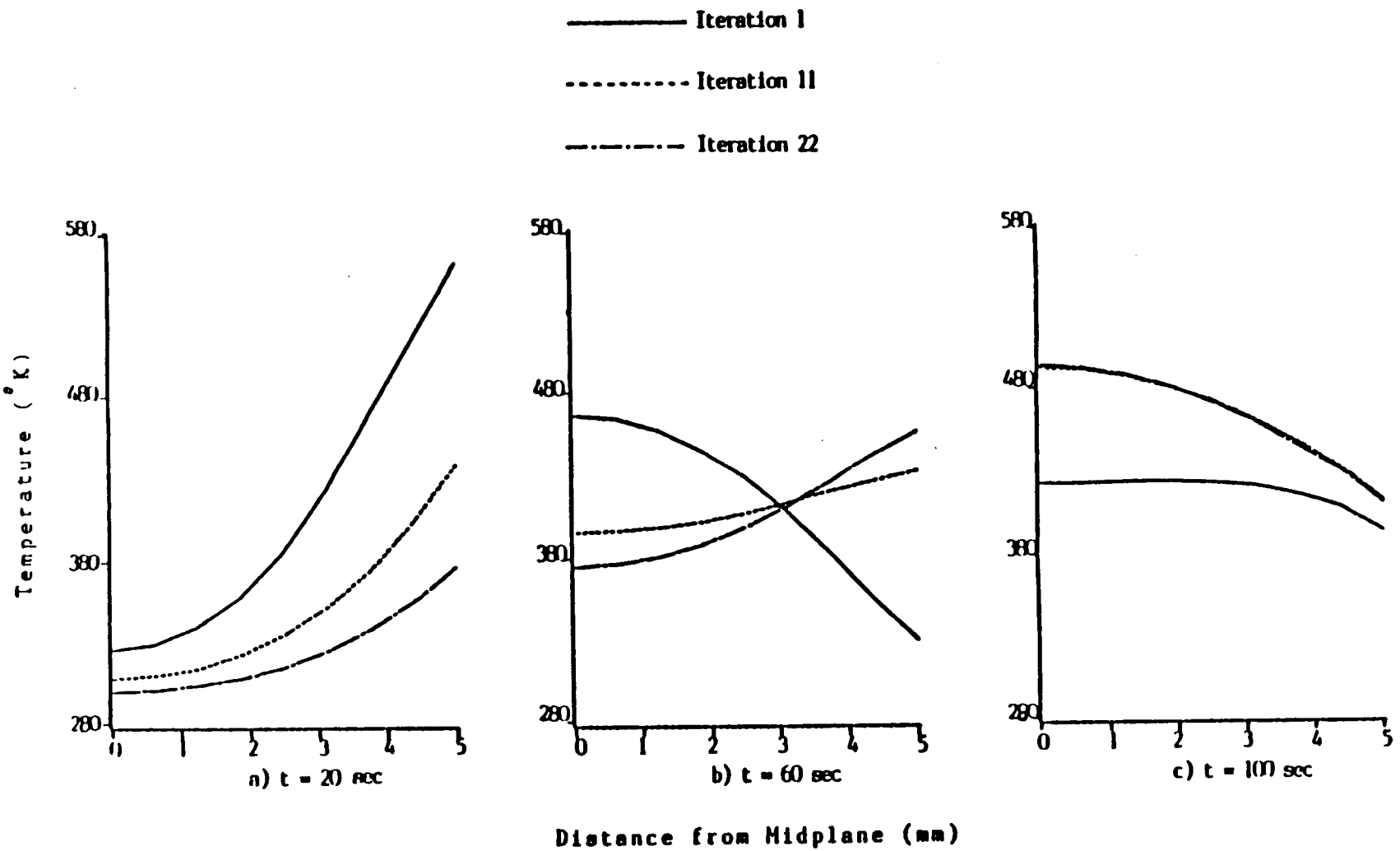

Figure 4.4 Example 1: Profiles of Temperature Distribution.

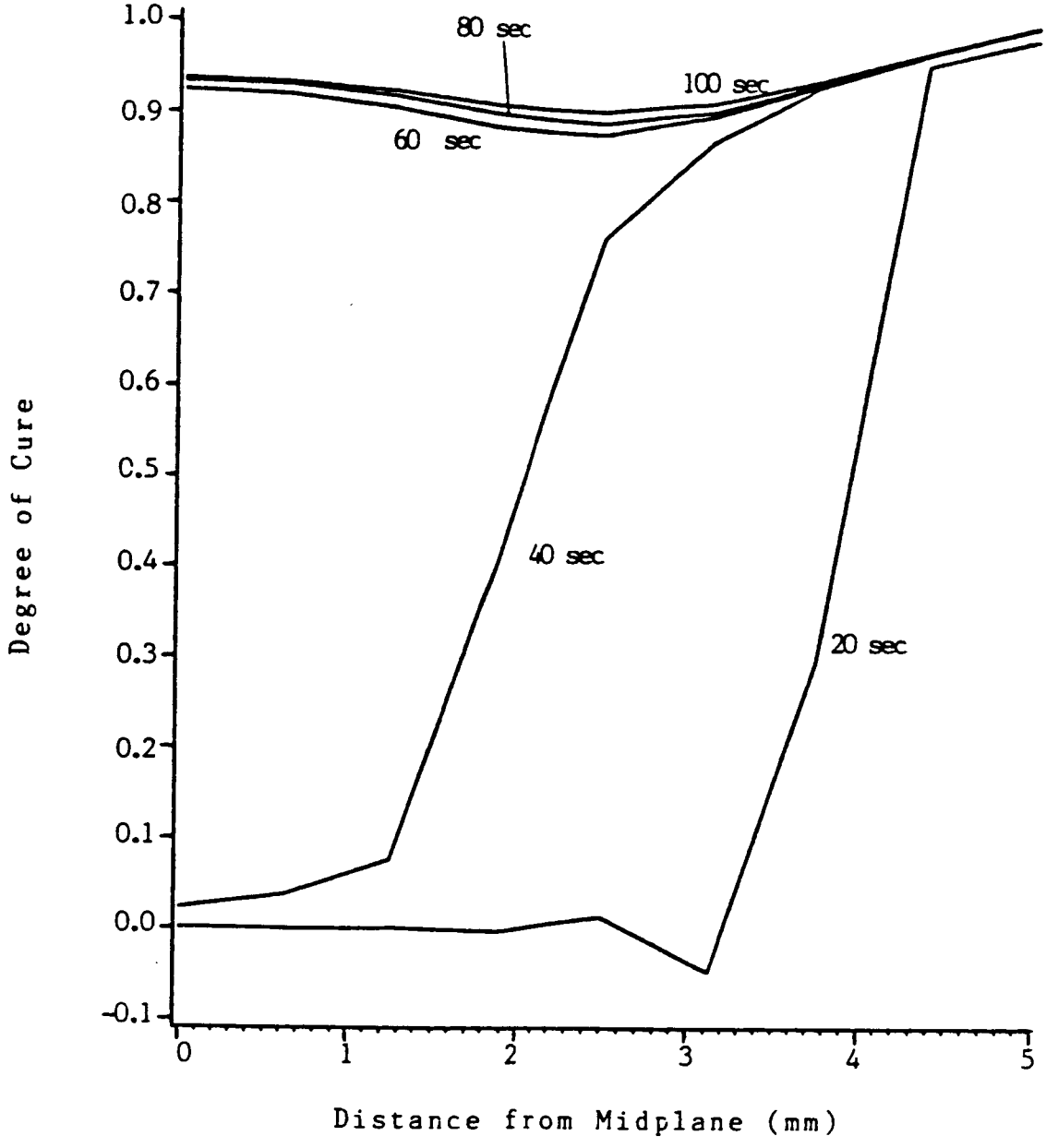

Figure 4.5 Example 1: The Degree of Cure Distribution at Iteration 1.

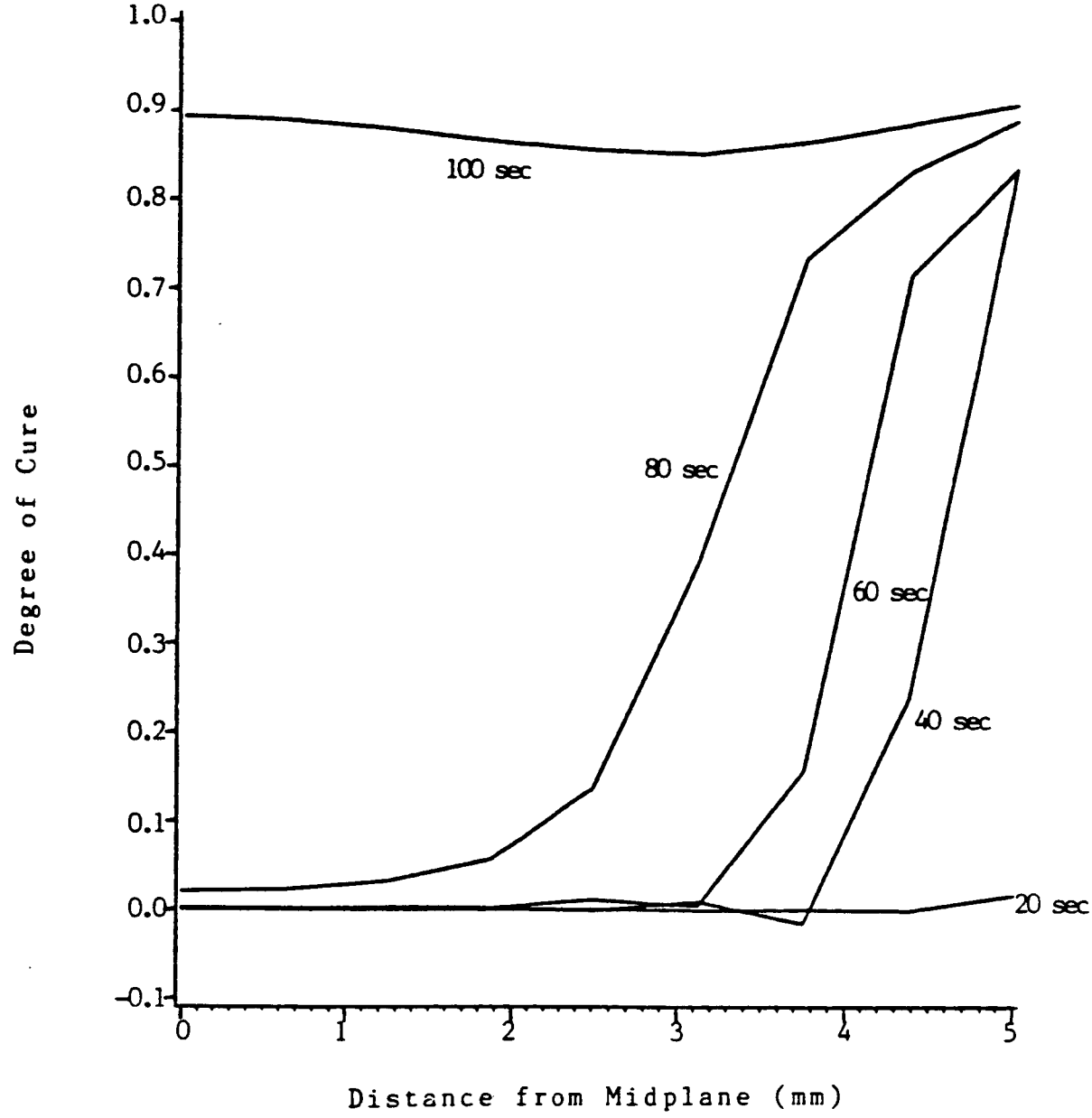

Figure 4.6 Example 1: The Degree of Cure Distribution at Interation 11.

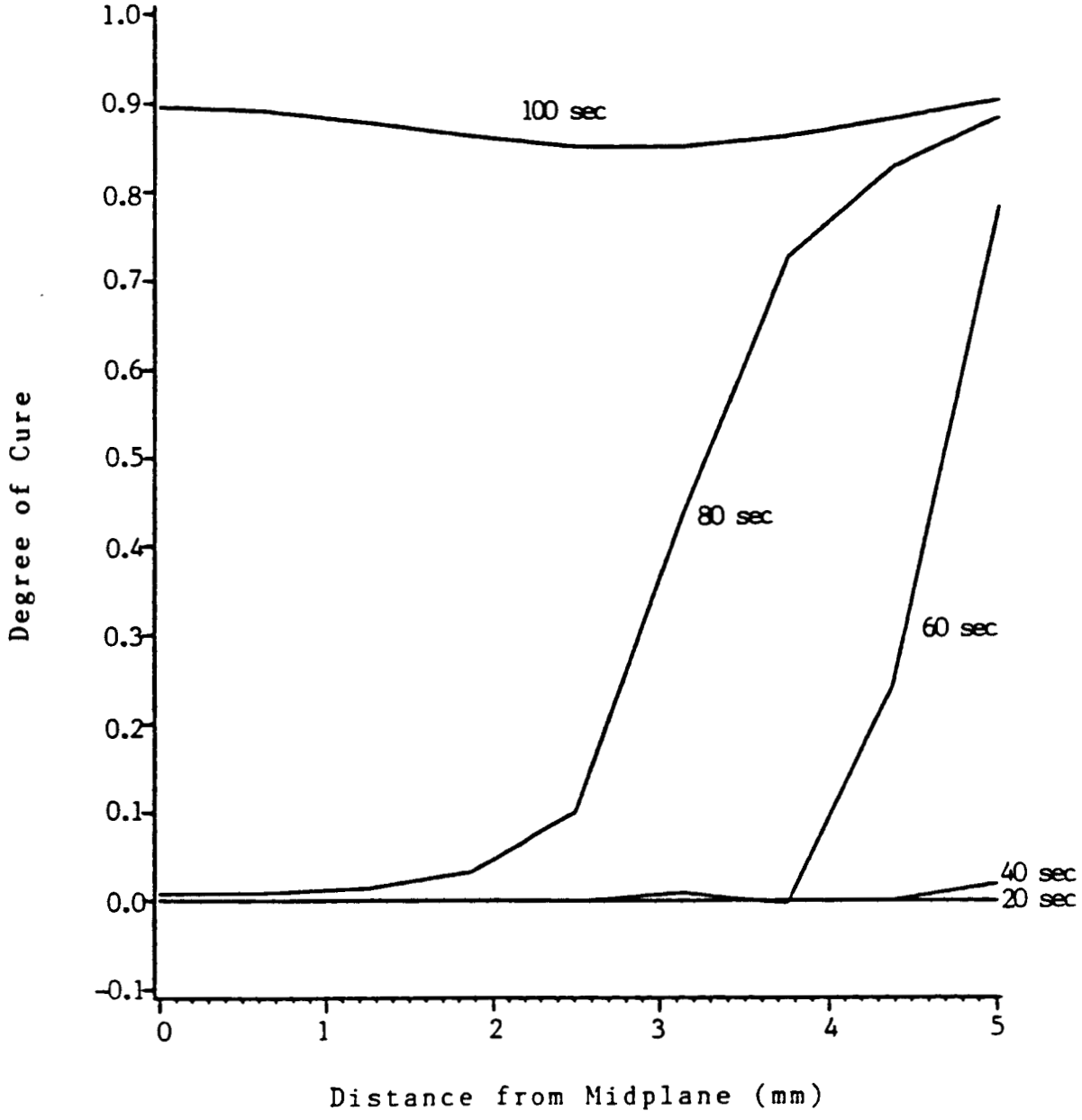

Figure 4.7 Example 1: The Degree of Cure Distribution at Iteration 22.

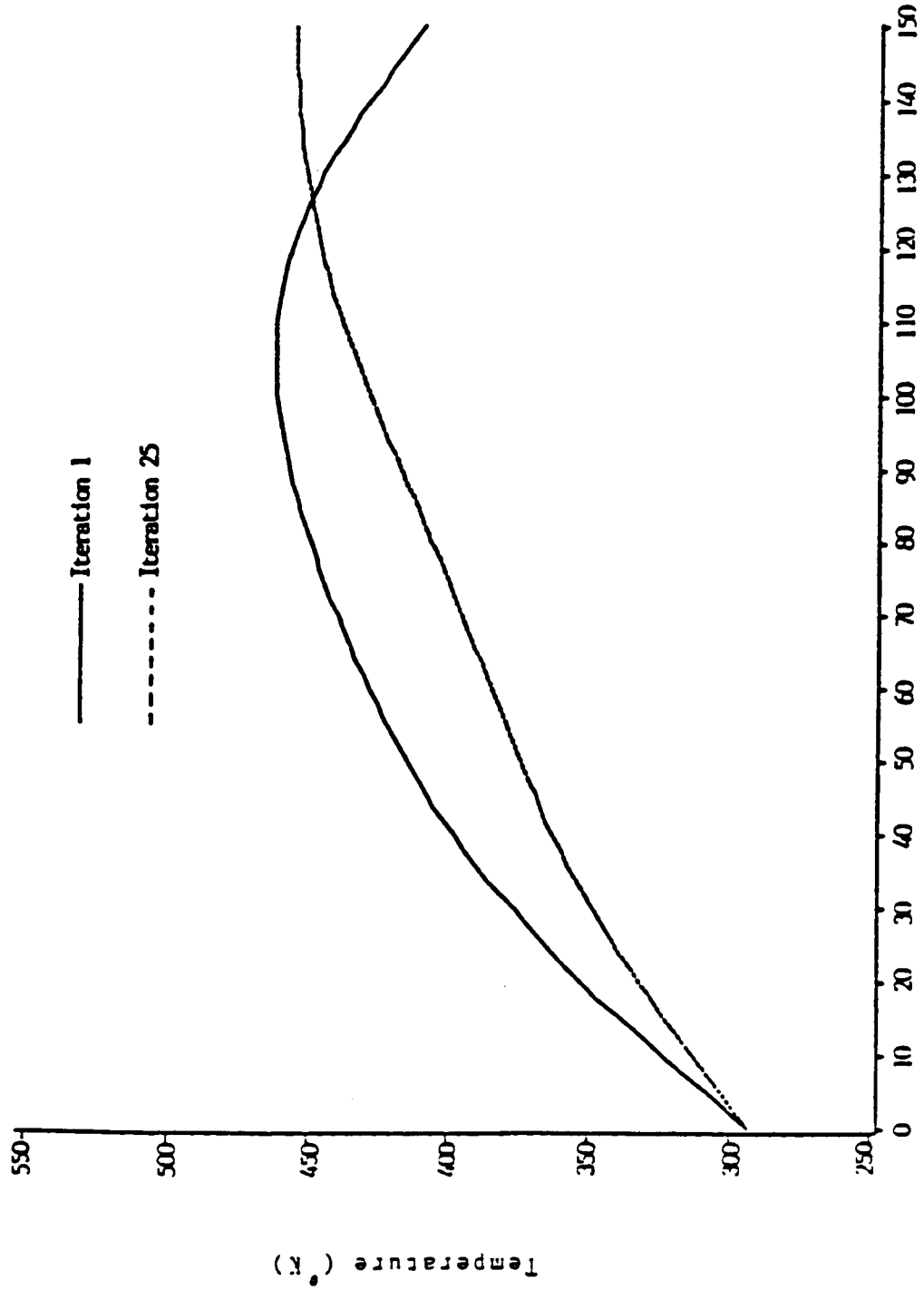

Figure 4.8 Example 2: Profiles of the Cure Temperature.

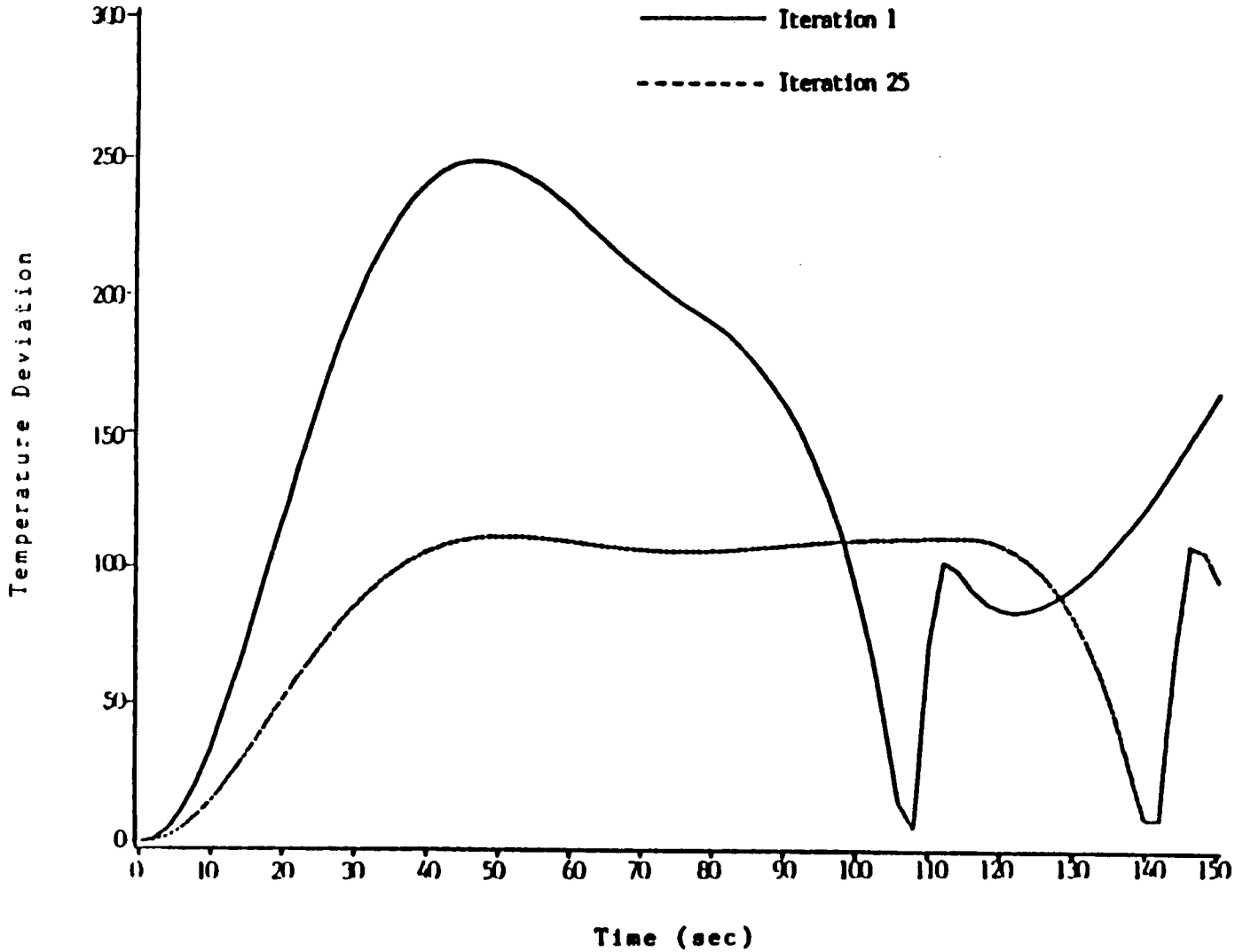

Figure 4.9 Example 2: Profiles of the Least Squared Temperature Deviation.

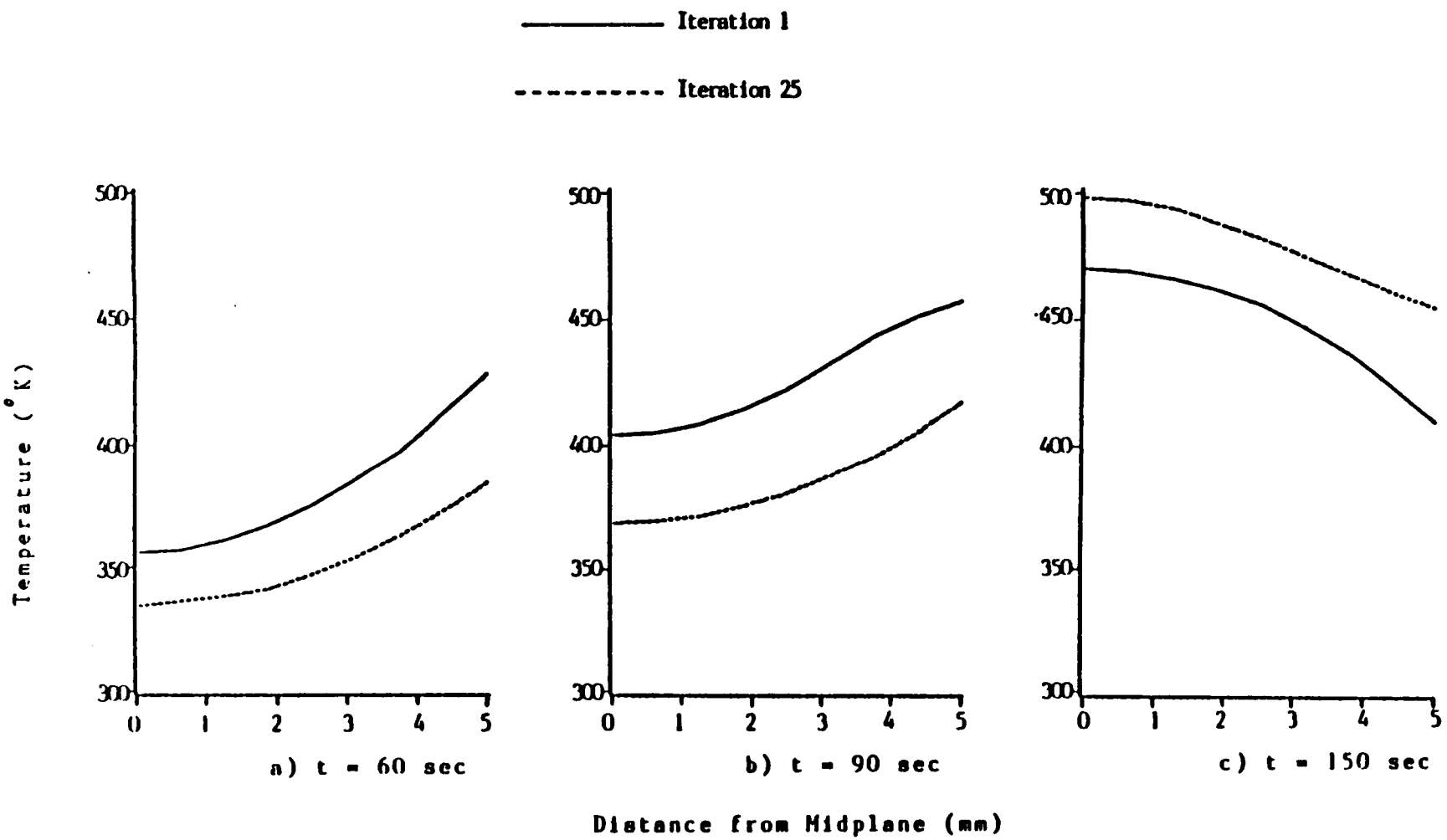

Figure 4.10 Example 2: Profiles of the Temperature Distribution.

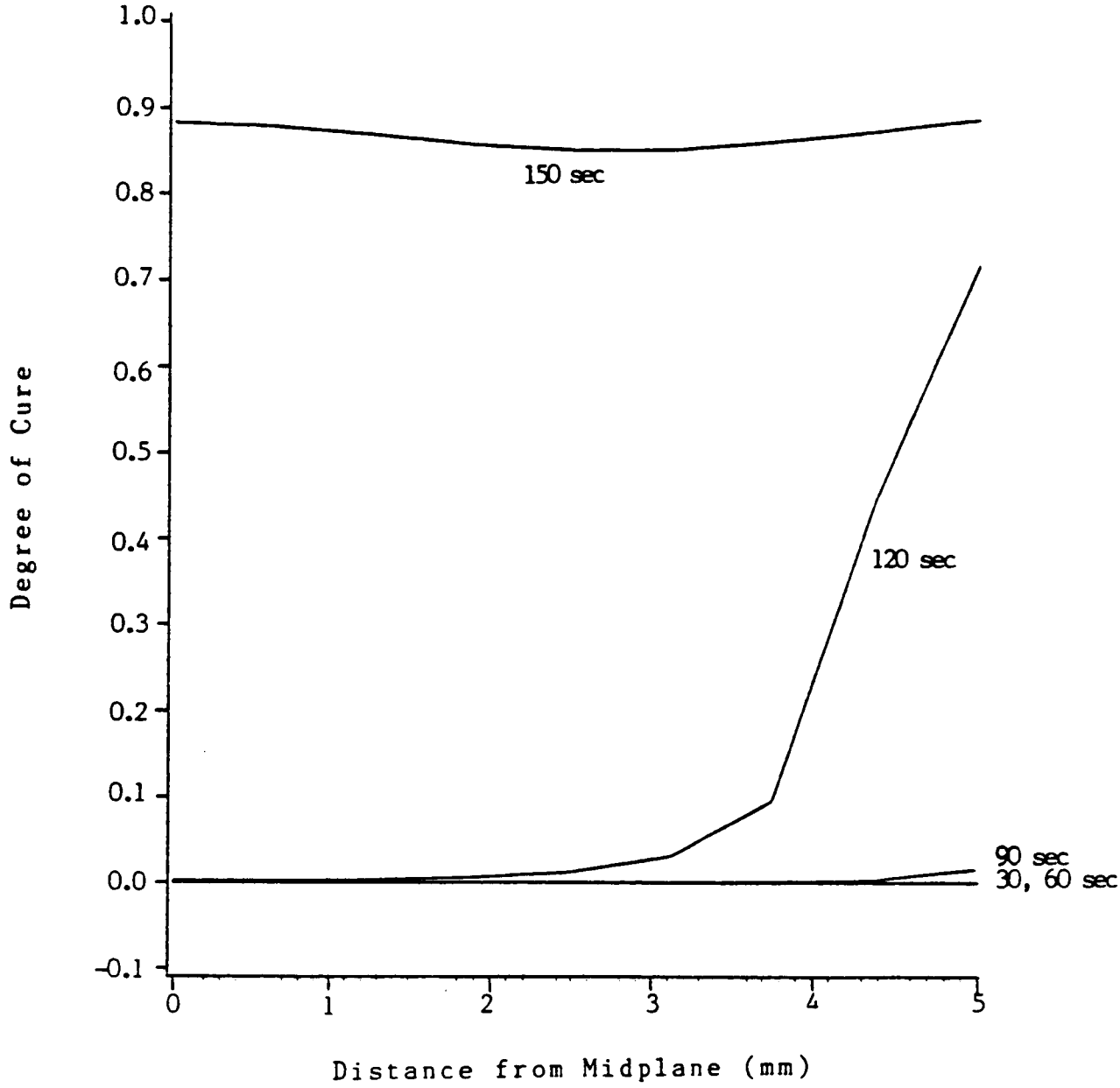

Figure 4.11 Example 2: The Degree of Cure Distribution at Iteration 25.

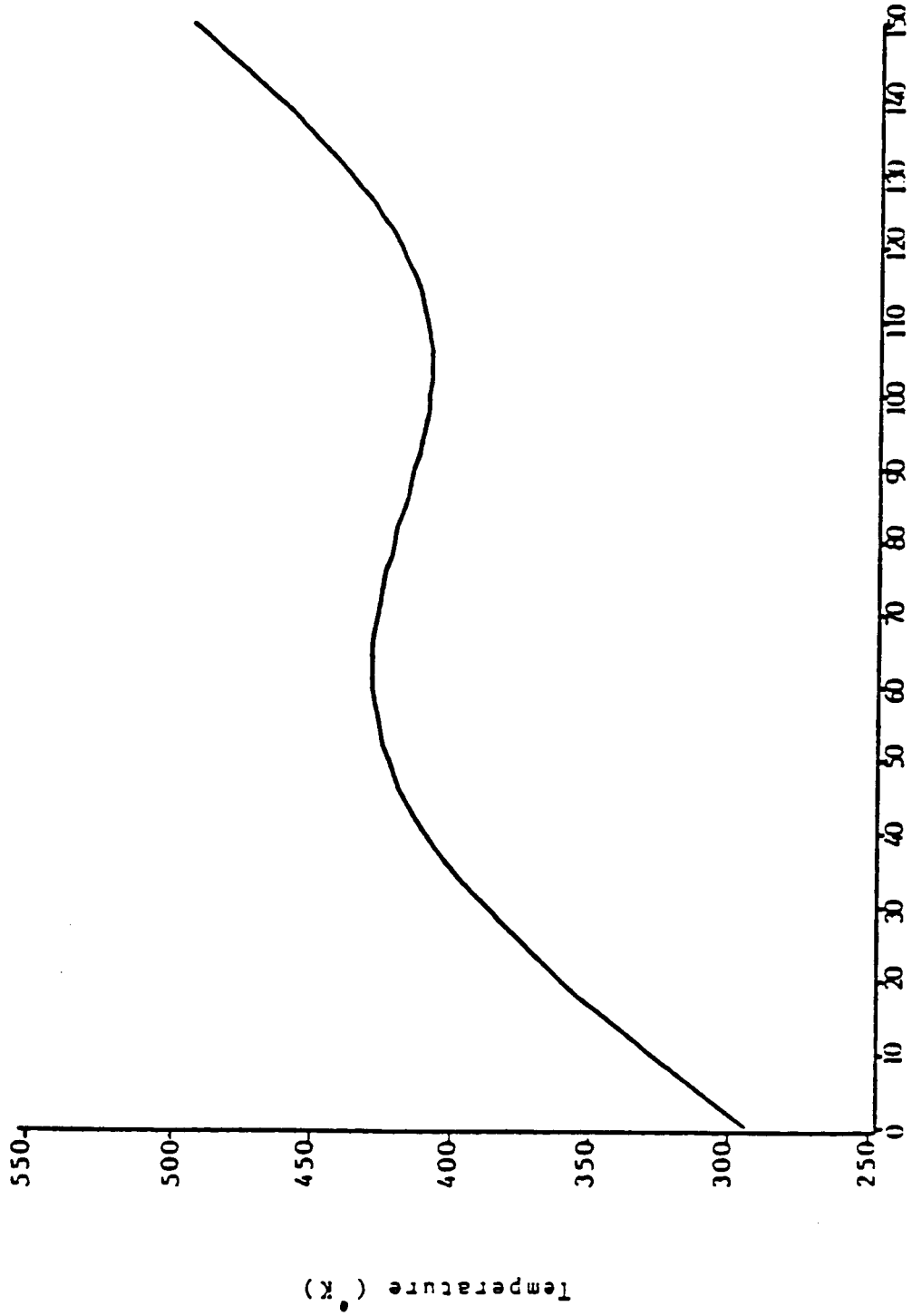

Figure 4.12 Example 3: Profile of the Optimal Cure Temperature at Iteration 55.

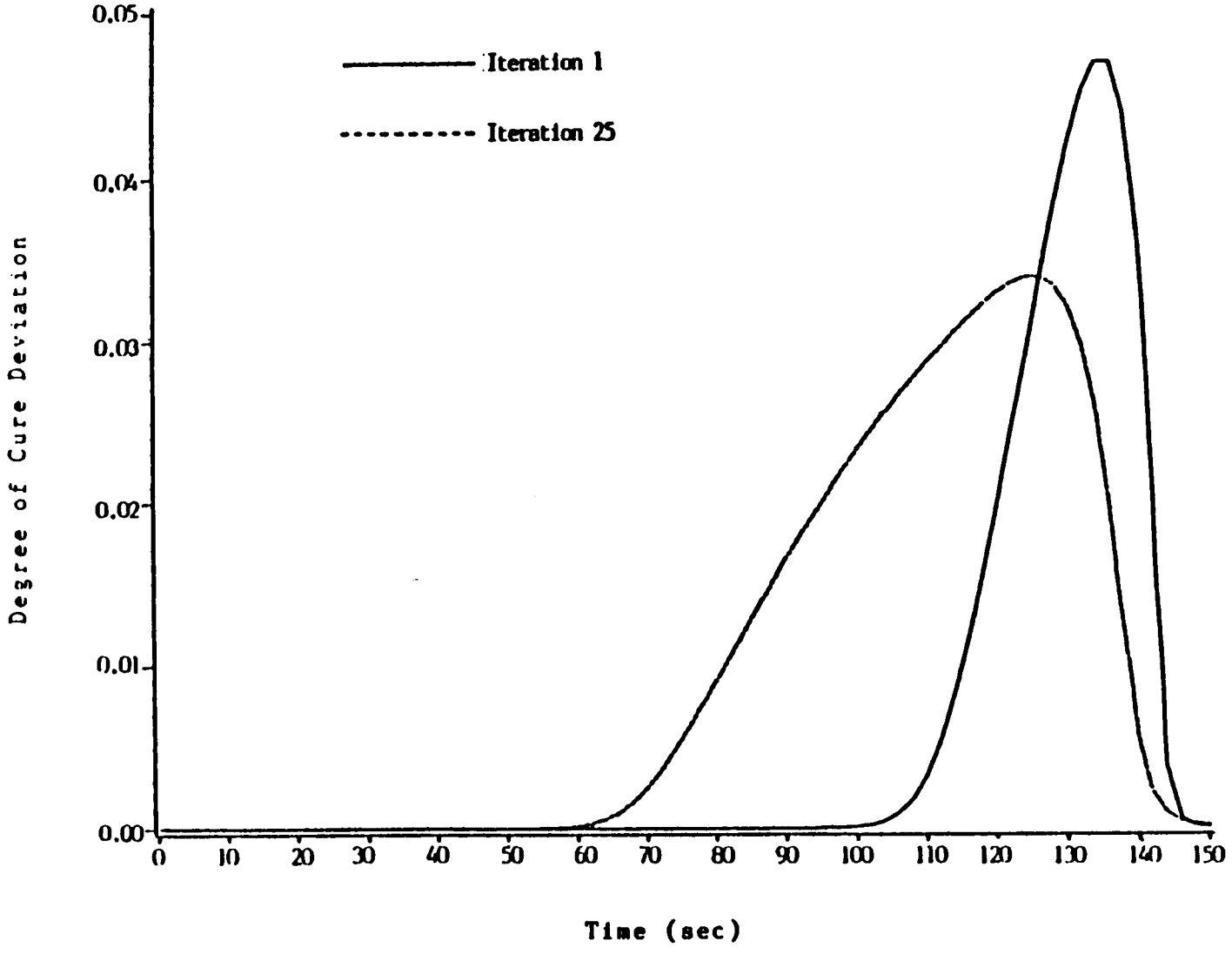

Figure 4.13 Example 3: Profiles of the Least-Squared Degree of Cure Deviation.

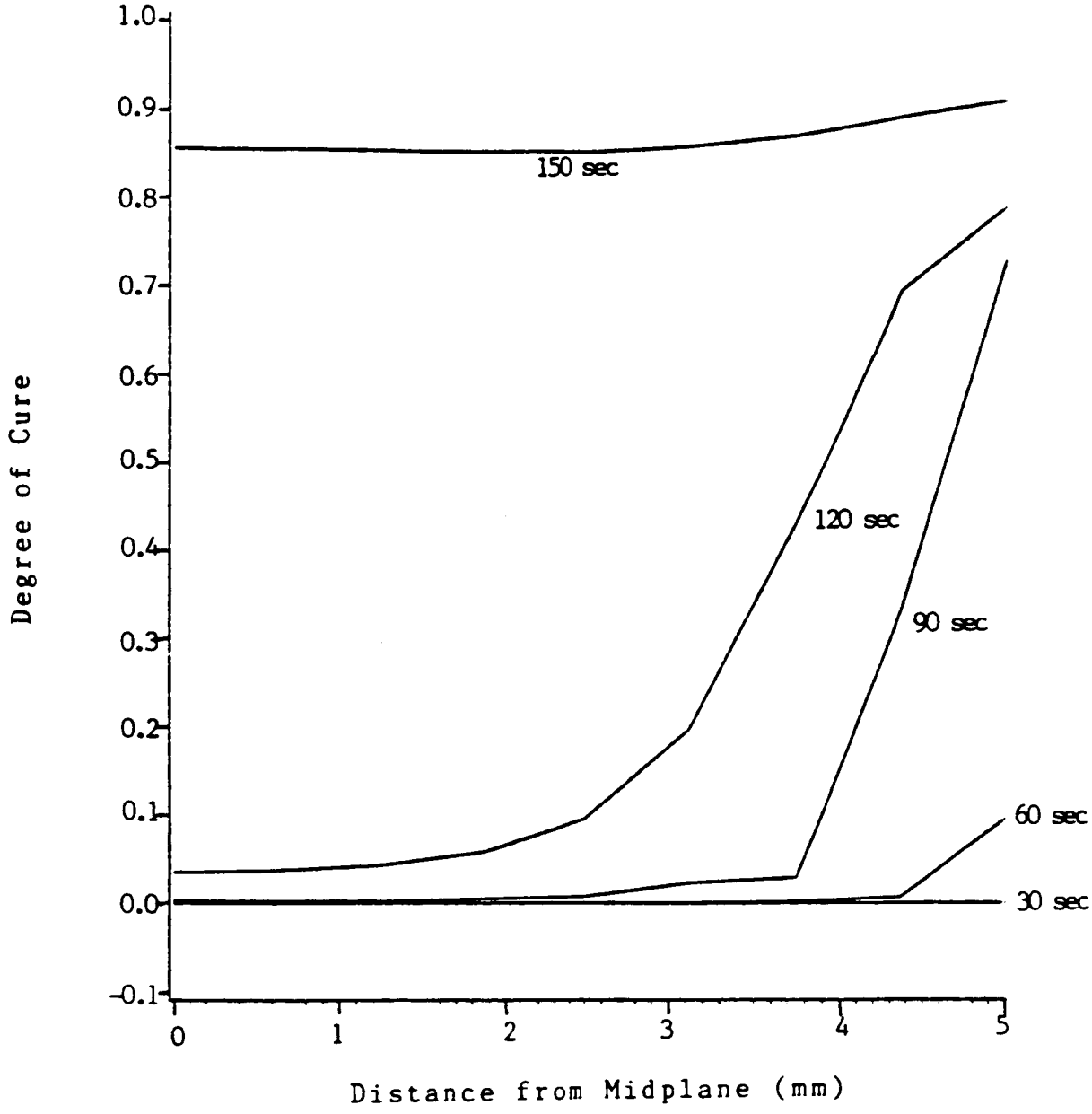

Figure 4.14 Example 3: The Degree of Cure Distribution at Iteration 55.

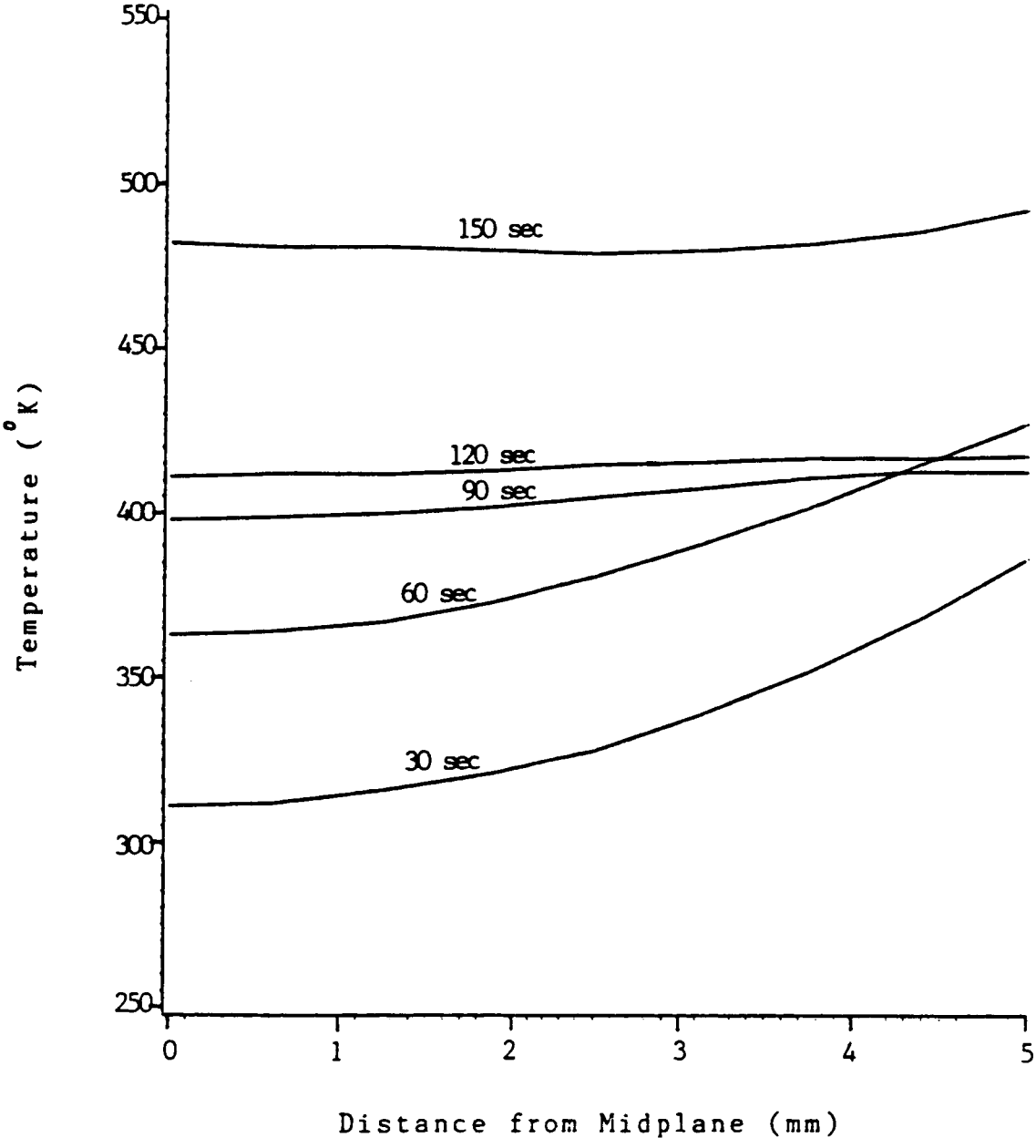

Figure 4.15 Example 3: The Temperature Distribution at Iteration 55.

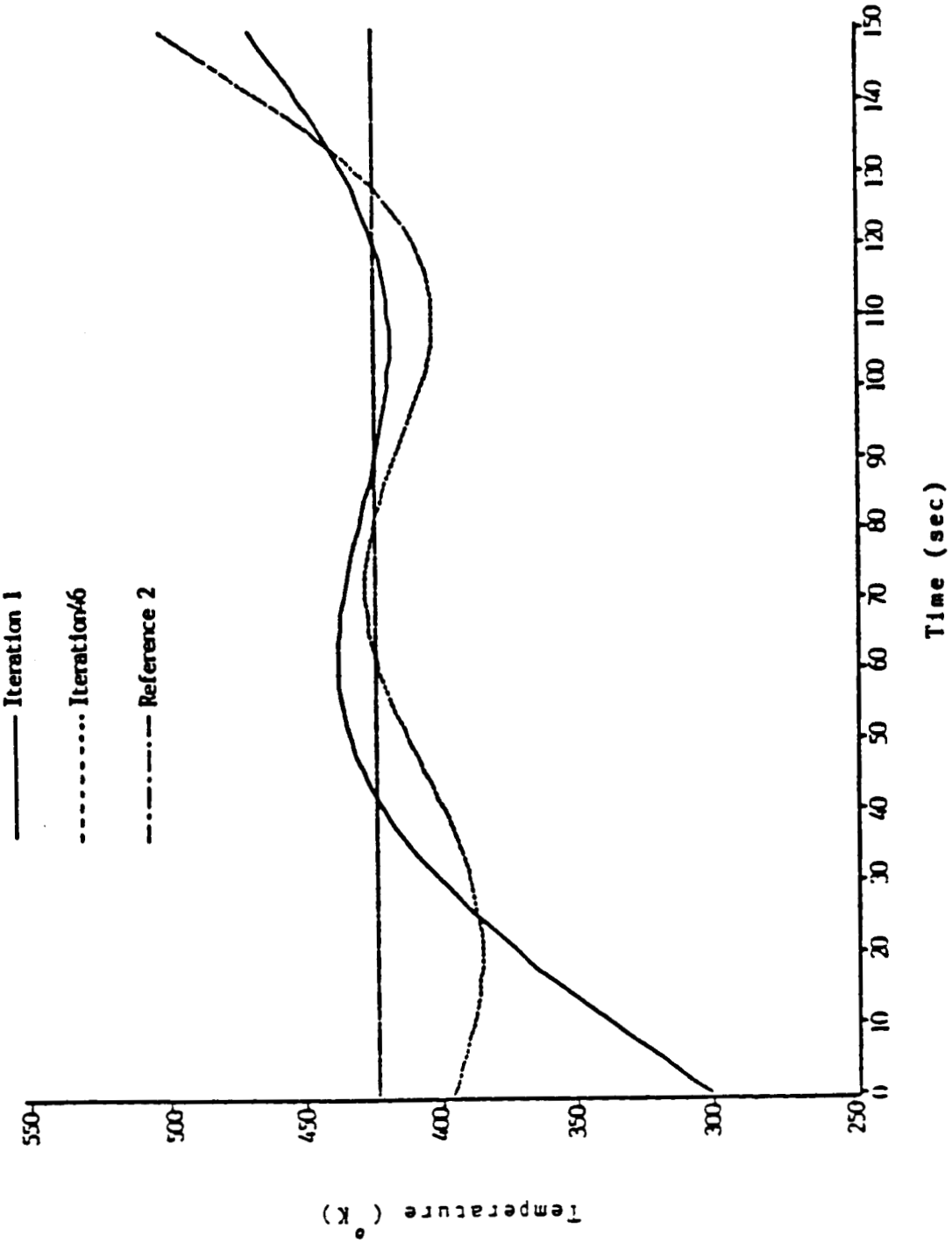

Figure 4.16 Example 4: Profiles of the Cure Temperature.

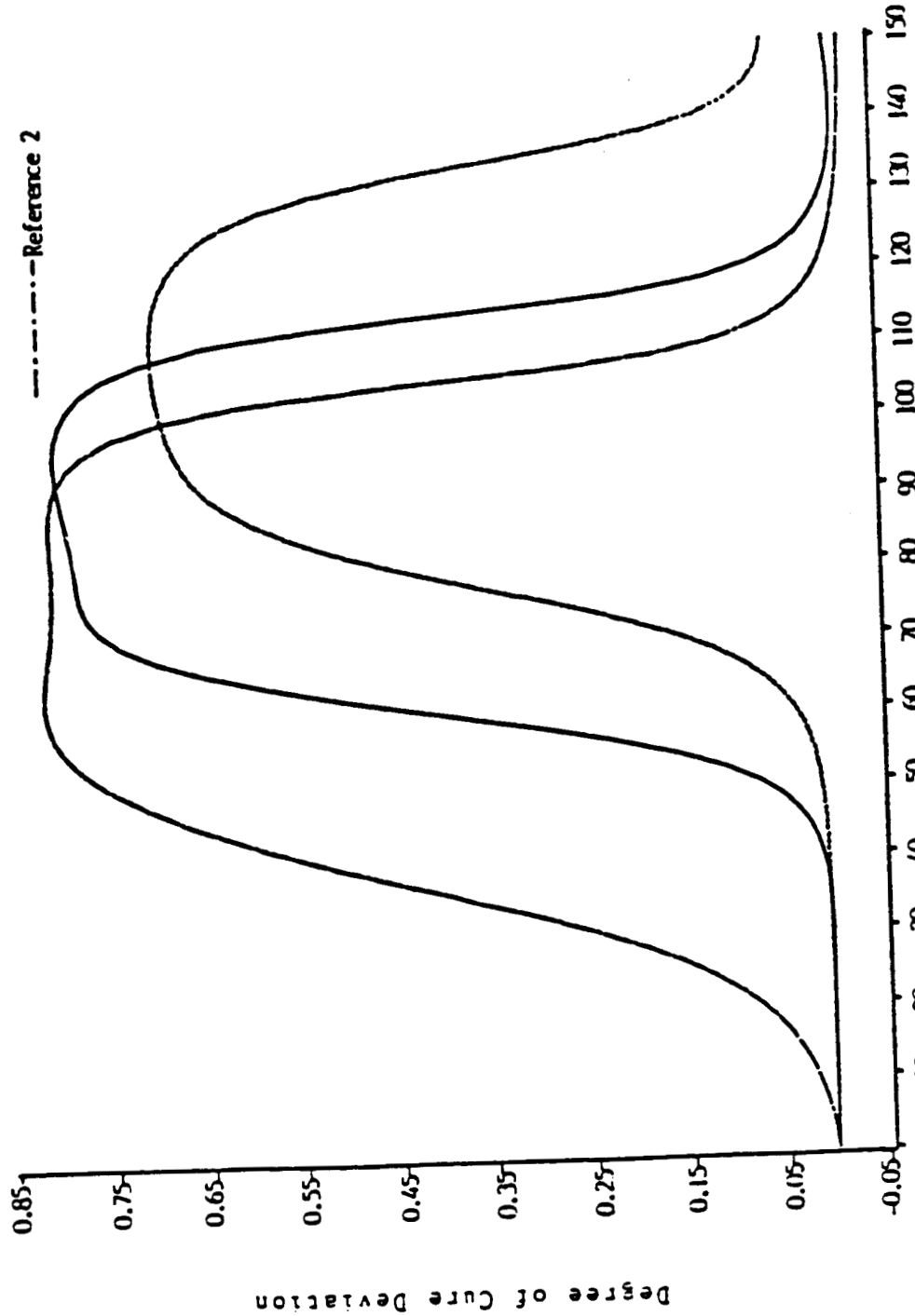

Figure 4.17 Example 4: Profiles of the Degree of Cure Deviation between the Outer Surface and the Center Plane of the Material.

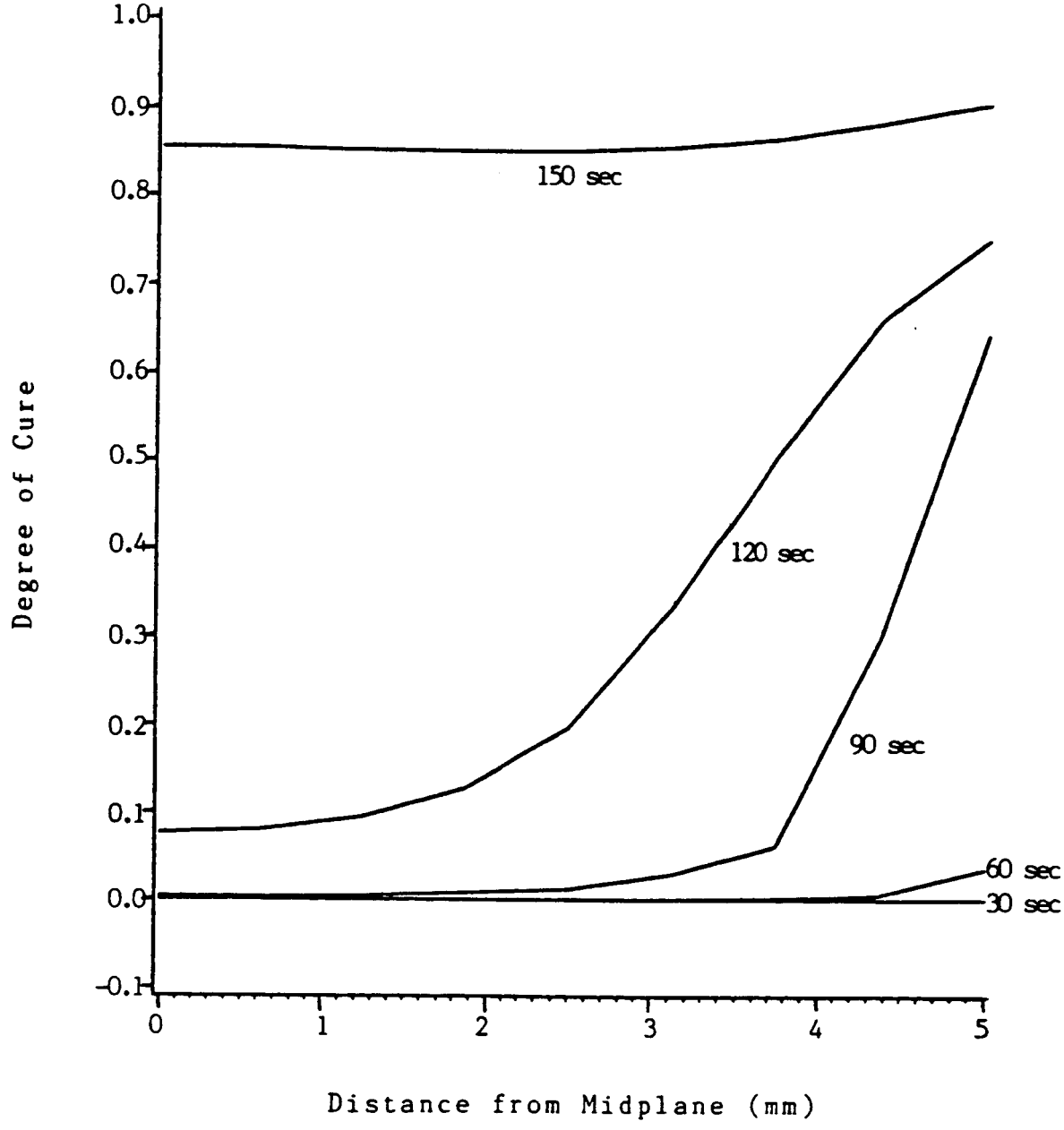

Figure 4.18 Example 4: The degree of Cure Distribution at Iteration 46.

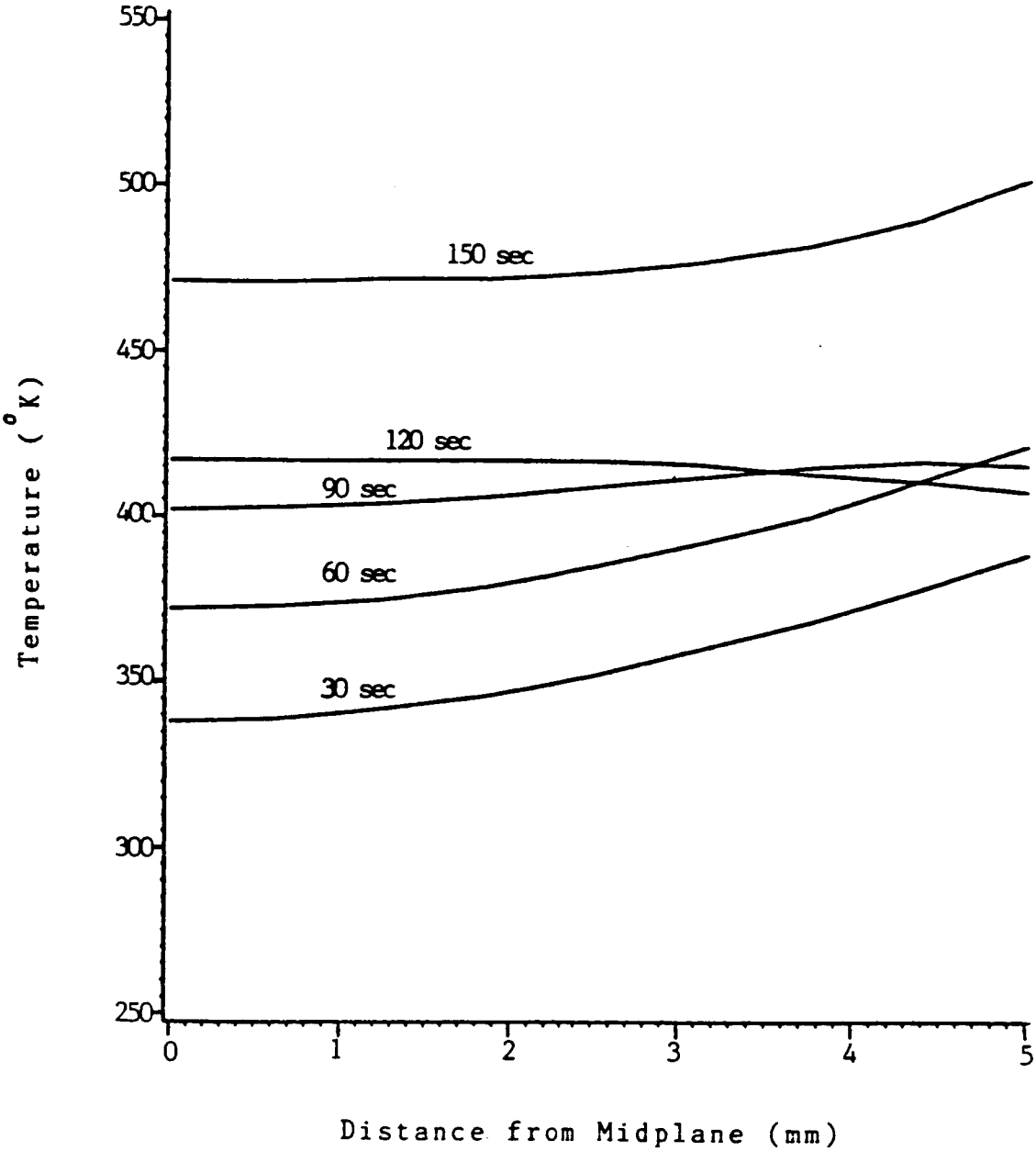

Figure 4.19 Example 4: The Temperature Distribution at Iteration 46.